Differentiable Solver Search for Fast Diffusion Sampling

Shuai Wang [1] **Zexian Li** [2] **Qipeng Zhang** [2] **Tianhui Song** [1] **Xubin Li** [2]
Tiezheng Ge [2] **Bo Zheng** [2] **Limin Wang** [1 3]

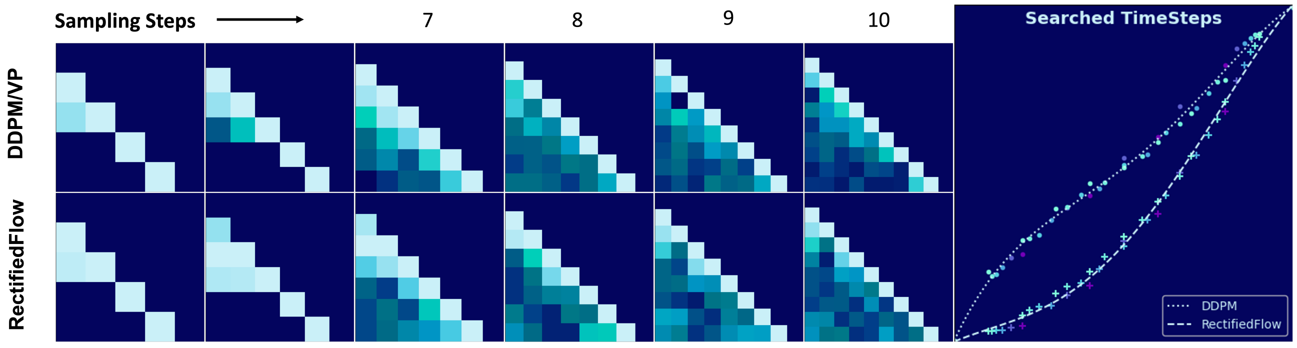

Figure 1: **Visualization of the searched solver parameters of DDPM/VP and Rectified Flow.** We limit the order of solver coefficients of the last two steps for 5/6 NFE. The left images show the absolute value of searched coefficients $\{c_i^j\}$. The right image shows the searched timesteps of different NFE and the fitted curves.

Abstract

Diffusion models have demonstrated remarkable generation quality, but at the cost of numerous function evaluations. Advanced ODE-based solvers have recently been developed to mitigate the substantial computational demands of reverse-diffusion solving under limited sampling steps. However, these solvers, heavily inspired by Adams-like multi-step methods, rely solely on t-related Lagrange interpolation. We show that t-related Lagrange interpolation is suboptimal for diffusion models and define a compact search space comprised of time steps and solver coefficients. Based on our analysis, we propose a new differentiable solver search algorithm to find a more optimal solver. Equipped with the searched solver, rectified-flow models, e.g., SiT-XL/2 and FlowDCN-XL/2, achieve FID scores of 2.40 and 2.35, respectively, on ImageNet-256×256 with only 10 steps. Meanwhile, DDPM model of DiT-XL/2 reaches a FID score of 2.33 with only 10 steps. Notably, our searched solver significantly outperforms the traditional solvers, even for some distillation-based methods. Moreover, our searched solver demonstrates generality across various model architectures, resolutions, and model sizes.

[1]State Key Lab of Novel Software Technology, Nanjing University, Nanjing, China. [2]Taobao & Tmall Group of Alibaba, Hangzhou, China. [3]Shanghai AI Lab, Shanghai, China.. Correspondence to: Limin Wang <lmwang@nju.edu.cn>.

Proceedings of the 42nd International Conference on Machine Learning, Vancouver, Canada. PMLR 267, 2025. Copyright 2025 by the author(s).

1. Introduction

Image generation is a fundamental task in computer vision, which aims at capturing the inherent data distribution of original image datasets and generating high-quality synthetic images through distribution sampling. Diffusion models (Ho et al., 2020; Song et al., 2020b; Karras et al., 2022; Liu et al., 2022; Lipman et al., 2022; Wang et al., 2025) have recently emerged as highly promising solutions to learn the underlying data distribution in image generation, outperforming GAN-based models (Brock et al., 2018; Sauer et al., 2022) and Auto-Regressive models (Chang et al., 2022) by a significant margin.

However, diffusion models necessitate numerous denoising steps during inference, which incur a substantial computational cost, thereby limiting their widespread deployment. The existing studies have explored two distinct approaches to achieve fast diffusion sampling. Training-based techniques by distilling the fast ODE trajectory into the model parameters, thereby circumventing redundant refinement steps. In addition, solver-based methods (Lu et al., 2023;

Zhang & Chen, 2023; Song et al., 2020a) tackle the fast sampling problem by designing high-order numerical ODE solvers.

For training-based acceleration, (Salimans & Ho, 2022) aligns the single-step student denoiser with the multi-step teacher output, thereby reducing inference burdens. The consistency model concept, introduced by (Song et al., 2023), directly teaches the model to produce consistent predictions at any arbitrary timesteps. Building upon (Song et al., 2023), subsequent works (Zheng et al., 2024; Kim et al., 2023; Wang et al., 2024a; Xu et al., 2024; Song et al., 2025) propose improved techniques to mitigate discrete errors in LCM training. Furthermore, (Lin et al., 2024; Kang et al., 2024; Yin et al., 2024; Zhou et al., 2024; Wang et al., 2023) leverage adversarial training and distribution matching to enhance the quality of generated samples. However, training-based methods introduce changes to the model parameters, resulting in an inability to exploit the power of pre-trained models fully.

Solver-based methods rely heavily on the ODE formulation in the reverse-diffusion dynamics and hand-crafted multi-step solvers. (Lu et al., 2023; 2022) and (Zhang & Chen, 2023) point out the semi-linear structure of the diffusion ODE and propose an exponential integrator to tackle faster sampling in diffusion models. (Zhao et al., 2023) further enhances the sampling quality by introducing the predictor-corrector structure. Thanks to the multistep-based ODE solver methods, high-quality samples can be generated within as few as 10 steps. To further improve efficiency, (Gao et al., 2023) tracks the backward error and determines the adaptive step. Moreover, (Karras et al., 2022; Lu et al., 2022) propose a handcrafted timesteps scheduler to sample respaced timesteps. (Xue et al., 2024) argues that timesteps sampled in (Karras et al., 2022; Lu et al., 2022) are suboptimal, thus proposing an online optimization algorithm to find the optimal sampling timesteps for generation. Apart from timesteps optimization, (Shaul et al., 2023) learns a specific path transition to improve the sampling efficiency.

In contrast to training-based acceleration methods, solver-based approaches do not necessitate parameter adjustments and are able to preserve the original performance of the pre-trained models. Moreover, solvers can be seamlessly applied to any arbitrary diffusion model trained with a similar noise scheduler, offering a high degree of flexibility and generality. This property enables us to investigate the generative capabilities of pre-trained diffusion models within limited steps from a diffusion solver perspective.

Current state-of-the-art diffusion solvers (Lu et al., 2023; Zhao et al., 2023) adopt Adams-like multi-step methods that use the Lagrange interpolation function to minimize integral errors. We argue that an optimal solver should be tailored to specific pre-trained denoising functions and their corresponding noise schedulers. In this paper, we present a new solver-based method for fast diffusion sampling by using data-driven approaches without destroying the pre-trained internality in diffusion models. Inspired by (Xue et al., 2024), we investigate the sources of error in the diffusion ODE and discover that the form of the interpolation function is inconsequential, which can be reduced to coefficients. Furthermore, we define a compact search space related to the timesteps and solver coefficients. Therefore, we propose a differentiable solver search method to identify the optimal parameters in this compact search space.

Based on our novel differentiable solver search algorithm, we investigate the upper bound performance of pre-trained diffusion models under limited steps. Our searched solver significantly improves the performance of pre-trained diffusion models, and outperforms traditional solvers with a large gap. On ImageNet-256×256, armed with our solver, rectified-flow models of SiT-XL/2 and FlowDCN-XL/2 achieve 2.40 and 2.35 FID, respectively, under 10 steps, while DDPM model of DiT-XL/2 achieves 2.33 FID. Surprisingly, our findings reveal that when equipped with an optimized high-order solver, the DDPM can perform comparably or even surpass the performance of rectified flow models under similar NFE constraints.

To summarize, our contributions are

- We reveal that the interpolation function choice is not important and can be reduced to coefficients through the pre-integral technique. We demonstrate that the upper bound of discretization error in reverse-diffusion ODE is related to both timesteps and solver coefficients. Thus, we define a compact solver search space.
- Based on our analysis, we propose a novel differentiable solver search algorithm to find the optimal solver parameter for given pre-trained diffusion models.
- For DDPM/VP time scheduling, armed with our searched solver, DiT-XL/2 achieves 2.33 FID under 10 steps, beating DPMSolver++/UniPC by a significant margin.
- For Rectified-flow models, armed with our searched solver, SiT-XL/2 and FlowDCN-XL/2 achieve 2.40 and 2.35 FID respectively under 10 steps on ImageNet-256×256.
- For Text-to-Image diffusion models like FLUX, SD3, PixArt-Σ, our solver searched on ImageNet-256×256 consistently yields better images compared to traditional solvers with the same CFG scale.

2. Related Work

Diffusion Model gradually adds $\boldsymbol{x}_0$ with Gaussian noise ϵ to perturb the corresponding known data distribution $p(x_0)$ into a simple Gaussian distribution. The discrete perturbation function at each step t satisfies $\mathcal{N}(\boldsymbol{x}_t|\alpha_t\boldsymbol{x}_0, \sigma_t^2\boldsymbol{I})$ as follows:

$$\boldsymbol{x}_t = \alpha_t\boldsymbol{x}_{\text{real}} + \sigma_t\boldsymbol{\epsilon}, \tag{1}$$

where $\alpha_t, \sigma_t > 0$. Moreover, as shown in Equation (2), Equation (1) has a forward continuous-SDE description, where $f(t) = \frac{\mathrm{d}\log\alpha_t}{\mathrm{d}t}$ and $g(t) = \frac{\mathrm{d}\sigma_t^2}{\mathrm{d}t} - \frac{\mathrm{d}\log\alpha_t}{\mathrm{d}t}\sigma_t^2$. (Anderson, 1982) establishes a pivotal theorem that the forward SDE has an equivalent reverse-time diffusion process as in Equation (3), so the generating process is equivalent to solving the diffusion SDE. Typically, diffusion models employ neural networks and distinct prediction parametrization to estimate the score function $\nabla\log_x p_{\boldsymbol{x}_t}(\boldsymbol{x}_t)$ along the sampling trajectory (Song et al., 2020b; Karras et al., 2022; Ho et al., 2020).

$$d\boldsymbol{x}_t = f(t)\boldsymbol{x}_t\mathrm{d}t + g(t)\mathrm{d}\boldsymbol{w}. \tag{2}$$

$$d\boldsymbol{x}_t = [f(t)\boldsymbol{x}_t - g(t)^2\nabla_{\boldsymbol{x}}\log p(\boldsymbol{x}_t)]dt + g(t)d\boldsymbol{w}. \tag{3}$$

(Song et al., 2020b) also shows that there exists a corresponding deterministic process Equation (4) whose trajectories share the same marginal probability densities of Equation (3) as follows:

$$d\boldsymbol{x}_t = [f(t)\boldsymbol{x}_t - \frac{1}{2}g(t)^2\nabla_{\boldsymbol{x}_t}\log p(\boldsymbol{x}_t)]dt. \tag{4}$$

Rectified Flow Model simplifies diffusion model under the framework of Equation (2) and Equation (3). Different from (Ho et al., 2020) introduces non-linear transition scheduling, the rectified-flow model adopts a linear function to transform data to standard Gaussian noise:

$$\boldsymbol{x}_t = t\boldsymbol{x}_{\text{real}} + (1-t)\boldsymbol{\epsilon}. \tag{5}$$

Instead of estimating the score function $\nabla_{\boldsymbol{x}_t}\log p_t(\boldsymbol{x}_t)$, rectified-flow models directly learn a neural network $v_\theta(x_t, t)$ to predict the velocity field $\boldsymbol{v}_t = d\boldsymbol{x}_t = (\boldsymbol{x}_{\text{real}} - \boldsymbol{\epsilon})$.

$$\mathcal{L}(\theta) = \mathbb{E}[\int_0^1 ||\boldsymbol{v}_\theta(\boldsymbol{x}_t, t) - \boldsymbol{v}_t||^2\mathrm{d}t]. \tag{6}$$

Solver-based Fast Sampling Method does not necessitate parameter adjustments and preserves the optimal performance of the pre-trained model. It can be seamlessly applied to an arbitrary diffusion model trained with a similar noise scheduler, offering a high degree of flexibility and adaptability. Solvers heavily rely on the reverse diffusion ODE in Equation (4). Current solvers are mainly focused on DDPM/VP noise schedules. (Lu et al., 2022; Zhang & Chen, 2023) discovered the semi-linear structure in DDPM/VP reverse ODEs. Furthermore, (Zhao et al., 2023) enhanced the sampling quality by borrowing the predictor-corrector structure. Thanks to the multi-step ODE solvers, high-quality samples can be generated within as few as 10 steps. To further improve efficiency, (Gao et al., 2023) tracks the backward error and determines the adaptive step. Moreover, (Karras et al., 2022; Lu et al., 2022) proposed a handcrafted timestep scheduler to sample respaced timesteps. However, (Xue et al., 2024; Sabour et al., 2024; Chen et al., 2024a) argued that the handcrafted timesteps are suboptimal, and thus proposed an online optimization algorithm to find the optimal sampling timestep for generation. Apart from timestep optimization, (Shaul et al., 2023) learned a specific path transition to improve the sampling efficiency.

3. Problem Definition

As rectified-flow has a simple yet elegant formulation within the diffusion family, we choose it as the primary subject of discussion in this paper to enhance readability. Importantly, our proposed algorithm is not constrained to rectified-flow models. We explore its applicability to other diffusion models such as DDPM/VP in Section 6.

Recall the continuous integration of reverse-diffusion in Equation (7) has the pre-defined interval $\{t_0, t_1, ...t_N\}$. Given the pre-trained diffusion models and their corresponding ODE defined in Equation (4), before we tackle the integration of interval $[t_i, t_{i+1}]$, we have already obtained the sampled velocity field of previous timestep $\{(\boldsymbol{x}_j, t_j, \boldsymbol{v}_j = \boldsymbol{v}_\theta(\boldsymbol{x}_j, t_j)\}_{j=0}^{i}$. Here, we directly denote $\boldsymbol{x}_{t_i}$ as $\boldsymbol{x}_i$ for presentation clarity:

$$\boldsymbol{x}_{i+1} = \boldsymbol{x}_i + \int_{t_i}^{t_{i+1}} \boldsymbol{v}_\theta(\boldsymbol{x}_t, t)dt. \tag{7}$$

As shown in Equation (8), we strive to develop **a more optimal solver** that minimizes the integral error while enhancing image quality under limited sampling steps (NFE) without requiring any parameter adjustments for the pre-trained model:

$$\Phi = \arg\min\mathbb{E}[||\Phi(\boldsymbol{\epsilon}, \boldsymbol{v}_\theta) - (\boldsymbol{\epsilon} + \int_0^1 \boldsymbol{v}_\theta(\boldsymbol{x}_t, t)dt)||]. \tag{8}$$

4. Analysis of reverse-diffusion ODE Sampling

Initially, we revisit the multi-step methods commonly used by (Zhao et al., 2023; Zhang & Chen, 2023; Lu et al., 2023) and identify potential limitations. Specifically, we argue that the Lagrange interpolation function used in Adams-Bashforth methods is suboptimal for diffusion models. Moreover, we show that the specific form of the interpolation function is inconsequential, as pre-integration and

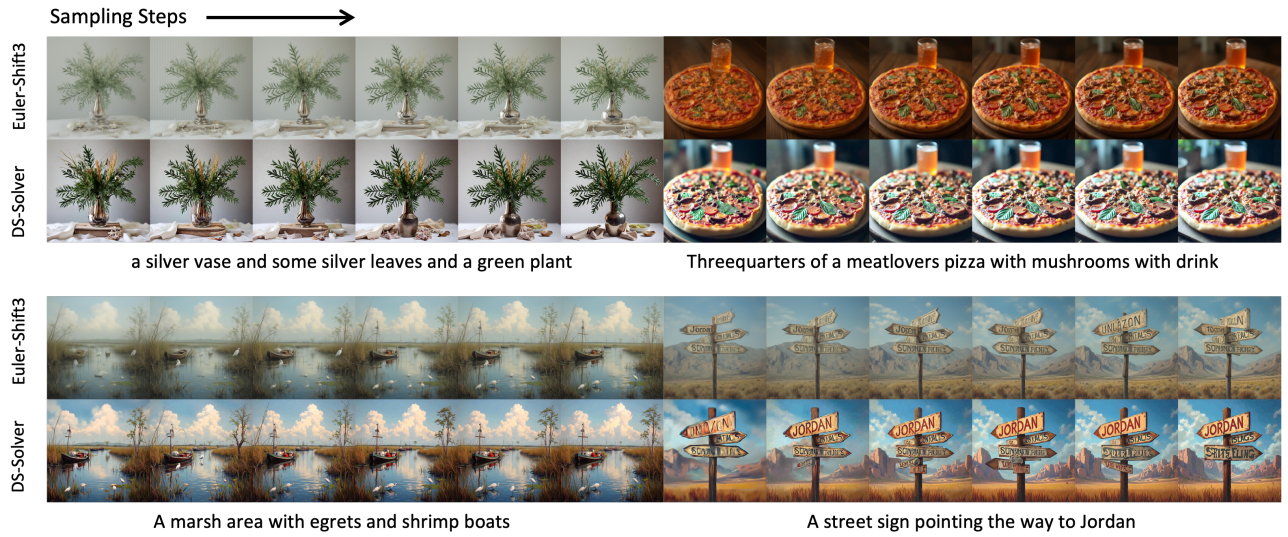
Sampling Steps
Euler-Shift3
DS-Solver
Euler-Shift3
DS-Solver
a silver vase and some silver leaves and a green plant
Threequarters of a meatlovers pizza with mushrooms with drink
A marsh area with egrets and shrimp boats
A street sign pointing the way to Jordan

Figure 2: **Generated images from Flux.1-dev with Guidance=2.0 and our solver (searched on SiT-XL/2).** Euler-Shift3 is the default solver provided by diffusers and Flux community. Our solver(DS-Solver) achieves better visual quality from 5 to 10 steps(NFE).

expectation estimation ultimately reduce it to a set of coefficients. Inspired by (Xue et al., 2024), we prove that timesteps and these coefficients effectively constitute our search space.

4.1. Revisit the multi-step methods

As shown in Equation (9), the Euler method employs $\boldsymbol{v}_i$ as an estimate of Equation (9) throughout the interval $[t_i, t_{i+1}]$. Higher-order multistep solvers further improve the estimation quality of the integral by incorporating interpolation functions and leveraging previously sampled values.

$$\boldsymbol{x}_{i+1} = \boldsymbol{x}_i + (t_{i+1} - t_i)\boldsymbol{v}_\theta(\boldsymbol{x}_i, t_i). \tag{9}$$

The most classic multi-step solver Adams–Bashforth method (Bashforth & Adams, 1883)(deemed as Adams for brevity) incorporates the Lagrange polynomial to improve the estimation accuracy within a given interval.

$$\boldsymbol{x}_{i+1} \approx \boldsymbol{x}_i + \int_{t_i}^{t_{i+1}} \sum_{j=0}^{i} (\prod_{k=0,k\neq j}^{i} \frac{t - t_k}{t_j - t_k}) \boldsymbol{v}_j dt. \tag{10}$$

$$\boldsymbol{x}_{i+1} \approx \boldsymbol{x}_i + \sum_{j=0}^{i} \boldsymbol{v}_j \int_{t_i}^{t_{i+1}} (\prod_{k=0,k\neq j}^{i} \frac{t - t_k}{t_j - t_k}) dt. \tag{11}$$

As Equation (11) states, $\int_{t_i}^{t_{i+1}} (\prod_{k=0,k\neq j}^{i} \frac{t-t_k}{t_j-t_k}) dt$ of the Lagrange polynomial can be pre-integrated into a constant coefficient, resulting in only naive summation being required for ODE solving. Current SoTA multi-step solvers (Lu et al., 2023; Zhao et al., 2023) are heavily inspired by Adams–Bashforth-like multi-step solvers. These solvers employ the Lagrange interpolation function or difference formula to estimate the value in the given interval.

However, the Lagrange interpolation function and other similar methods only take t into account while the $\boldsymbol{v}(\boldsymbol{x}, t)$ also needs $\boldsymbol{x}$ as inputs. Using first-order Taylor expansion of $\boldsymbol{x}$ at $\boldsymbol{x}_i$ and higher-order expansion of t at t_i, we can readily derive the error bound of the estimation.

4.2. Focus on solver coefficients instead of the interpolation function

In contrast to typical problems of solving ordinary differential equations, when considering reverse-diffusion ODEs along with pretrained models, a compact searching space is present. We define a universal interpolation function $\mathcal{P}$, which has no explicit form. $\mathcal{P}$ measures the distance of $(\boldsymbol{x}_t, t)$ between previous sampled points $\{(\boldsymbol{x}_j, t_j)\}_{j=0}^{i}$ to determine the interpolation weight for $\{\boldsymbol{v}_j\}_{j=0}^{i}$.

$$\boldsymbol{x}_{i+1} \approx \boldsymbol{x}_i + \int_{t_i}^{t_{i+1}} \sum_{j=0}^{i} \mathcal{P}(\boldsymbol{x}_t, t, \boldsymbol{x}_j, t_j) \boldsymbol{v}_j dt. \tag{12}$$

$$\approx \boldsymbol{x}_i + \sum_{j=0}^{i} \boldsymbol{v}_j \int_{t_i}^{t_{i+1}} \mathcal{P}(\boldsymbol{x}_t, t, \boldsymbol{x}_j, t_j) dt. \tag{13}$$

Assumption 4.1. We assume that the remainder term of the universal interpolation function $\sum_{j=0}^{i} \mathcal{P}(\boldsymbol{x}_t, t, \boldsymbol{x}_j, t_j)\boldsymbol{v}_j$ for $v(\boldsymbol{x}, t)$ is bound as $\mathcal{O}(d\boldsymbol{x}^m) + \mathcal{O}(dt^n)$, where $\mathcal{O}(d\boldsymbol{x}^m)$ is the mth-order infinitesimal for $d\boldsymbol{x}$, $\mathcal{O}(dt^m)$ is the nth-order infinitesimal for dt.

Equation (13) has a recurrent dependency, as $\boldsymbol{x}_t$ also relies on $\sum_{j=0}^{i} \mathcal{P}(\boldsymbol{x}_t, t, \boldsymbol{x}_j, t_j)\boldsymbol{v}_j dt$. To eliminate the recurrent dependency, shown in Equation (14), we simply use the first order Taylor expansion of $x(t)$ at x_i to replace the original form. Recall that $\boldsymbol{v}_i$ is already determined by $\boldsymbol{x}_i$ and t_i, thus the partial integral of Equation (14) can be formulated as Equation (15). Unlike naive Lagrange interpolation, $\mathcal{C}_j(\boldsymbol{x}_i)$ is a function of the current $\boldsymbol{x}_i$ instead of a constant scalar. Learning a $\mathcal{C}_j(\boldsymbol{x}_i)$ function will cause the generalization to be lost. This limits the actual usage in diffusion model sampling.

$$\boldsymbol{x}_{i+1} \approx \boldsymbol{x}_i + \sum_{j=0}^{i} \boldsymbol{v}_j \int_{t_i}^{t_{i+1}} \mathcal{P}(\boldsymbol{x}_i + \boldsymbol{v}_i(t - t_i), t, \boldsymbol{x}_j, t_j)dt. \tag{14}$$

$$\boldsymbol{x}_{i+1} \approx \boldsymbol{x}_i + \sum_{j=0}^{i} \boldsymbol{v}_j \mathcal{C}_j(\boldsymbol{x}_i)(t_{i+1} - t_i). \tag{15}$$

Theorem 4.2. *Given sampling time interval* $[t_i, t_{i+1}]$ *and suppose* $\mathcal{C}_j(\boldsymbol{x}_i) = g_j(\boldsymbol{x}_i) + b_i^j$, *Adams-like linear multi-step methods have an error expectation of* $(t_{i+1} - t_i)\mathbb{E}_{\boldsymbol{x}_i}||\sum_{j=0}^{i} \boldsymbol{v}_j g_j(\boldsymbol{x}_i)||$. *replacing* $\mathcal{C}_j(\boldsymbol{x})$ *with* $\mathbb{E}_{\boldsymbol{x}_i}[\mathcal{C}_j(\boldsymbol{x}_i)]$ *is the optimal choice and owns an error expectation of* $(t_{i+1} - t_i)\mathbb{E}_{\boldsymbol{x}_i}||\sum_{j=0}^{i} \boldsymbol{v}_j [g_j(\boldsymbol{x}_i) - \mathbb{E}_{\boldsymbol{x}_i} g_j(\boldsymbol{x}_i)||$. *We place the proof in Appendix H.*

According to Theorem 4.2, we opt to replace $\mathcal{C}_j(\boldsymbol{x}_i)$ with its expectation $\mathbb{E}_{\boldsymbol{x}_i}[\mathcal{C}_j(\boldsymbol{x}_i)]$, thus we obtain diffusion-scheduler-related coefficients while maintaining generalization ability.

Finally, given the predefined time intervals, we obtain the optimization target Equation (16), where $c_i^j = \mathbb{E}_{\boldsymbol{x}_i}[\mathcal{C}_j(\boldsymbol{x}_i)]$. The expectation can be deemed as optimized through massive data and gradient descent.

$$\boldsymbol{x}_{i+1} \approx \boldsymbol{x}_i + \sum_{j=0}^{i} \boldsymbol{v}_j c_i^j (t_{i+1} - t_i). \tag{16}$$

4.3. Search optimal solver

Assumption 4.3. As shown in Equation (17), the pre-trained velocity model $\boldsymbol{v}_\theta$ is not perfect and the error between $\boldsymbol{v}_\theta$ and ideal velocity field $\hat{\boldsymbol{v}}$ is L1-bounded, where η is a constant scalar.

$$||\hat{\boldsymbol{v}} - \boldsymbol{v}_\theta|| \leq \eta \ll ||\hat{\boldsymbol{v}}||. \tag{17}$$

Previous discussions assume we have a perfect velocity function. However, the ideal velocity is hard to obtain; we only have pre-trained velocity models. Following Equation (16), we can expand Equation (16) from $t_{i=0}$ to $t_{i=N}$ to obtain the error bound caused by non-ideal velocity estimation.

Theorem 4.4. *The error caused by the non-ideal velocity estimation model can be formulated in the following equation. We can employ triangle inequalities to obtain the error-bound(L1) of* $||\boldsymbol{x}_N - \hat{x}_N||$, *the proof can be found in the Appendix I.*

$$||\boldsymbol{x}_N - \hat{x}_N|| \leq \eta \sum_{i=0}^{N-1} \sum_{j=0}^{i} |c_i^j (t_{i+1} - t_i)|.$$

Based on Theorem 4.4, since the error bound is related to timesteps and solver coefficients, we can define a much more compact search space consisting of $\{c_i^j\}_{j<i, j=0, i=1}^{N}$ and $\{t_i\}_{i=0}^{N}$.

Theorem 4.5. *Based on Theorem 4.4 and Theorem 4.2. We can derive the total upper error bound(L1) of our solver search method and other counterparts.*

The total upper error bound of our solver search is:

$$\sum_{i=0}^{N-1} (t_{i+1} - t_i)(\sum_{j=0}^{i} \eta |\mathbb{E}_{\boldsymbol{x}_i} g_j(\boldsymbol{x}_i) + b_i^j|.$$
$$+ \mathbb{E}_{\boldsymbol{x}_i} ||\sum_{j=0}^{i} \boldsymbol{v}_j g_j(\boldsymbol{x}_i) - \mathbb{E}_{\boldsymbol{x}_i} g_j(\boldsymbol{x}_i)||).$$

Compared to Adams-like linear multi-step methods. Our searched solver has a small upper error bound. The proof can be found in the Appendix I.

Through Theorem 4.5, our searched solvers own a relatively small upper error bound. Thus, we can theoretically guarantee optimal compared to Adams-like methods.

5. Differentiable Solver Search

Through previous discussion and analysis, we identify $\{c_i^j\}_{j<i, j=0, i=1}^{N}$ and $\{t_i\}_{i=0}^{N}$ as the target search items. To this end, we propose a differentiable data-driven solver search approach to determine these searchable items.

Timestep Parametrization. As shown in Algorithm 1, we employ unbounded parameters $\{r_i,\}_{i=0}^{N-1}$ as the optimization subject, as the integral interval is from 0 to 1, we convert r_i into time-space deltas Δt_i with softmax normalization function to force their summation to 1. We can access timestep t_{i+1} through $t_{i+1} = t_i + \Delta t_i$. We initialize $\{r_i\}_{i=0}^{N-1}$ with 1.0 to obtain a uniform timestep distribution.

Coefficients Parametrization. Inspired by (Xue et al., 2024). Given Equation (16) and Equation (7), when the velocity field $v_\theta(x, t)$ yields constant value, an implicit constraint $\sum_{k=0}^{i} c_k^i = 1$ emerges. This observation motivates us to re-parameterize the diagonal value of M as $\{1 - \sum_{j=0}^{i-1} c_i^j,\}_{i=0}^{N-1}$. We initialize $\{c_i^k,\}$ with zeros to mimic the behavior of the Euler solver.

Algorithm 1 Solver Parametrization

```
**Requires:** $\{r_i,\}$ and $\{c_i^j,\}$
**TimeDeltas:** $\Delta t_0, \Delta t_1, ..., \Delta t_{n-1}$.
**SolverCoefficients:** $\mathcal{M} \in R^{N\times N}$
$\{\Delta t_i,\}$=Softmax($\{r_i\}$)
$\mathcal{M} = \begin{bmatrix} 1 & & & \\ c_1^0 & 1-c_1^0 & & \\ \vdots & \vdots & \vdots & \ddots \\ c_{n-1}^0 & c_{n-1}^1 & \cdots & 1-\sum_{k=0}^{n-1} c_{n-1}^k \end{bmatrix}$
```

Algorithm 2 Differentiable Solver Search

```
**Require:** $\boldsymbol{v}_\theta$ model, $\{\Delta t_i,\}_{i=0}^{N-1}$, $\mathcal{M}$, A buffer $Q$.
Compute $\{\tilde{\boldsymbol{x}}_l,\}_{l=0}^{L} = \textbf{Euler}(\boldsymbol{\epsilon}, v_\theta)$ .
**for** $i = 0$ **to** $N-1$ **do**
    $Q \overset{\text{buffer}}{\leftarrow} \boldsymbol{v}_\theta(\boldsymbol{x}_{t_i}, t_i)$
    Compute $\boldsymbol{v} = \sum_{j=0}^{i} \mathcal{M}_{ij} Q_j$.
    $t_{i+1} = t_i + \Delta t_i$
    $\boldsymbol{x}_{t_{i+1}} = \boldsymbol{x}_{t_i} + \boldsymbol{v}\Delta t_i$
**end for**
**return:** $\tilde{\boldsymbol{x}}_{t_{n-1}}, \mathcal{L}(\{\tilde{\boldsymbol{x}}_l\}_{l=0}^{L}, \{\boldsymbol{x}_i\}_{i=0}^{N})$
```

Mono-alignment Supervision. We take the L-step Euler solver's ODE trajectory $\{\tilde{\boldsymbol{x}}\}_{l=0}^{L}$ as reference. We minimize the gap between the target and source trajectories with the MSE loss. We also adopt Huber loss as auxiliary supervision for $\boldsymbol{x}_{t_N}$.

6. Extending to DDPM/VP framework

Applying our differentiable solver search to DDPM is infeasible. However, (Song et al., 2020b) suggests that there exists a continuous SDE process with $\{f(t) = -\frac{1}{2}\beta_t; g(t) = \sqrt{\beta_t}\}$ corresponding to discrete DDPM. This motivates us to transform the search space from the infeasible discrete space to its continuous SDE counterpart. (Lu et al., 2022) and (Zhang & Chen, 2023) discover the semi-linear structure of diffusion and propose exponential integral with ϵ parametrization to tackle the fast sampling problem of DDPM models, where $\alpha_t = e^{\int_0^t -\frac{1}{2}\beta_s ds}$, $\sigma_t = \sqrt{1 - e^{\int_0^t -\beta_s ds}}$ and $\lambda_t = \log \frac{\alpha_t}{\sigma_t}$. (Lu et al., 2023) further discovers that x parametrization is more powerful for diffusion sampling under limited steps, where $\bar{\boldsymbol{x}} = \frac{\boldsymbol{x}_t - \sigma\boldsymbol{\epsilon}}{\alpha_t}$.

$$\boldsymbol{x}_t = \frac{\sigma_t}{\sigma_s}\boldsymbol{x}_s + \sigma_t \cdot \int_{\lambda_s}^{\lambda_t} e^{\lambda} \bar{\boldsymbol{x}}_\theta(\boldsymbol{x}_{t(\lambda)}, t(\lambda)) \mathrm{d}\lambda. \tag{18}$$

We opt to follow the $\bar{x}$ parametrization as DPM-Solver++. However, we find directly interpolating $e^{\lambda}\boldsymbol{x}_\theta(x_t, t)$ as a whole part is hard for searching, and yields worse results. To avoid conflating the interpolation coefficients with exponential integral, we employ $\omega_t = \frac{\alpha_t}{\sigma_t}$ and transform Equation (18) into Equation (19) with a similar interpolation format as Equation (15), where $t(\omega)$ maps ω to timestep.

$$\boldsymbol{x}_t \approx \frac{\sigma_t}{\sigma_s}\bar{\boldsymbol{x}}_s + \sigma_t(\omega_t - \omega_s) \sum_{k=1}^{i} c_i^k \boldsymbol{x}_\theta(\bar{\boldsymbol{x}}_k, t_k) \tag{19}$$

7. Experiment

We demonstrate the efficiency of our differentiable solver search by conducting experiments on publicly available diffusion models. Specifically, we utilize DiT-XL/2 (Peebles & Xie, 2023) trained with DDPM scheduling and rectified-flow models SiT-XL/2 (Ma et al., 2024) and FlowDCN-XL/2 (Wang et al., 2024b). Our default training setting employs the Lion optimizer (Chen et al., 2024c) with a constant learning rate of 0.01 and no weight decay. We sample 50,000 images for the entire search process. Notably, searching with 50,000 samples using FlowDCN-B/2 requires approximately 30 minutes on 8 × H20 computation cards. During the search, we deliberately avoid using CFG to construct reference and source trajectories, thereby preventing misalignment.

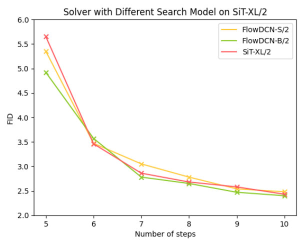

(a) FID of Search Model

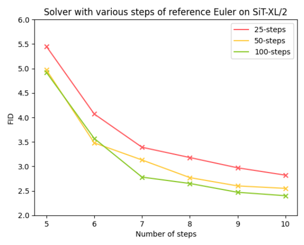

(b) FID of RefTraj Steps

Figure 3: **Ablations studies of Differentiable Solver Search.** We evaluate the searched solver on SiT-XL/2, and report the FID performance curve of searched solvers.

7.1. Rectified flow models

We search solvers with FlowDCN-B/2, FlowDCN-S/2 and SiT-XL/2. We compare the search solver's performance with the second-order and fourth-order Adam multistep method on SiT-XL/2, FlowDCN-XL/2 trained on ImageNet 256 × 256, and FlowDCN-XL/2 trained on ImageNet 512 × 512.

Search Model. We tried different search models among different sizes and architectures. We report the FID performance of SiT-XL/2 in Figure 3a. Surprisingly, we find that the FID performance of SiT-XL/2 equipped with the solver searched using FlowDCN-B/2 outperforms the solver searched on SiT-XL/2 itself. The reconstruction error(in the Appendix) between the sampled result produced by Euler-250 steps is as expected. These findings suggest that there exists a minor discrepancy between FID and the pursuit of

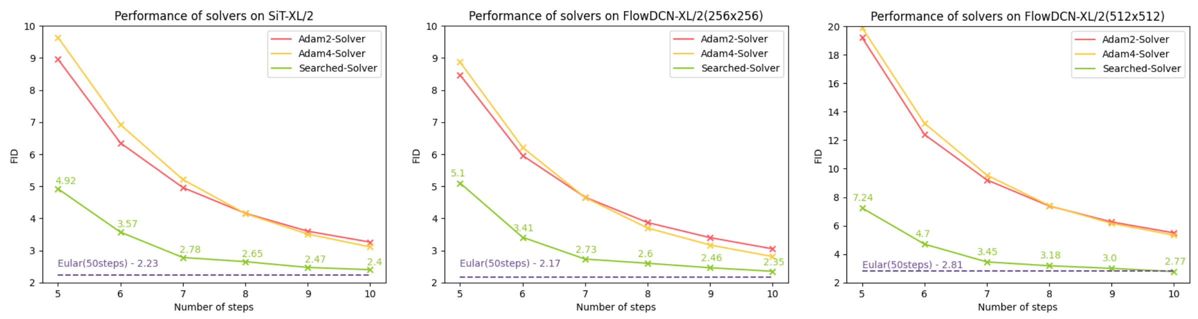

(a) SiT-XL/2-R256 (b) FlowDCN-XL/2-R256 (c) FlowDCN-XL/2-R512

Figure 4: **The same searched solver on different Rectified-Flow Models.** R256 and R512 indicate the generation resolution of given model. We search solver with FlowDCN-B/2 on ImageNet-256 $\times$ 256 and evaluate it with SiT-XL/2 and FlowDCN-XL/2 on different resolution datasets. Our searched solver outperforms traditional solvers by a significant margin. More metrics(sFID, IS, Precision, Recall) are places at Appendix

minimal error in the current solver design.

Step of Reference Trajectory. We provide reference trajectory $\{\tilde{x}\}_{l=0}^{L}$ of different sampling step L for differentiable solver search. We take FlowDCN-B/2 as the search model and report the FID measured on SiT-XL/2 in Figure 3b. As the sampling step of the reference trajectory increases, the FID of SiT-XL/2 further improves and becomes better. However, the performance improvement is not significant when the number of steps is 5 or 6, which suggests that there is a limit to the improvement achievable with an extremely small number of steps.

ImageNet 256×256**.** We validate the searched solver on SiT-XL/2 and FlowDCN-XL/2. We arm the pre-trained model with CFG of 1.375. As shown in Figure 4a, our searched solver improves FID performance significantly and achieves 2.40 FID under 10 steps. As shown in Figure 4b, our searched solver achieves 2.35 FID under 10 steps, beating traditional solvers by large margins.

We also provide the comparison with recent solver-based distillation (Zhao et al., 2024) to demonstrate the efficiency of our searched solver in Table 1. Our searched solver achieves better metric performance under similar NFE with fewer parameters.

SiT-XL-R256	NFE-CFG	Params	FID	IS
Heun	16x2	0	3.68	/
Heun	22x2	0	2.79	/
Heun	30x2	0	2.42	/
Adam2	15x2	/	2.49	236
Adam2	16x2	0	2.42	237
Adam4	15x2	/	2.33	242
Adam4	16x2	0	2.27	243
FlowTurbo	(7+3)x2	2.9×10^7	3.93	224
FlowTurbo	(8+2)x2	2.9×10^7	3.63	/
FlowTurbo	(12+2)x2	2.9×10^7	2.69	/
FlowTurbo	(17+3)x2	2.9×10^7	2.22	248
ours	6x2	21	3.57	214
ours	7x2	28	2.78	229
ours	8x2	36	2.65	234
ours	10x2	55	2.40	238
ours	15x2	55	2.24	244

Table 1: **Comparison with the distillation-based methods.** Our searched solver achieves much better result under the same NFE with much fewer parameters.

ImageNet 512×512**.** Since (Ma et al., 2024) has not released SiT-XL/2 trained on 512×512 resolution, we directly report the performance collected from FlowDCN-XL/2. We arm FlowDCN-XL/2 with CFG of 1.375 and four channels. Our searched solver achieves 2.77 FID under 10 steps, beating traditional solver by a large margin, even slightly outperforming the Euler solver with 50 steps(2.81FID).

Text to Image. Shown in Figure 2, we apply our solver search on FlowDCN-B/2 and SiT-XL/2 to the most advanced Rectified-Flow model Flux.1-dev and SD3 (Esser et al., 2024). We find Flux.1-Dev would produce grid points in generation. To alleviate the grid pattern, we decouple the velocity field into mean and direction, only apply our solver to the direction, and replace the mean with an exponential decayed mean. The details can be found in the appendix.

We also provide the result of distillation on SD1.5 and SDXL with solver search in Appendix F.

7.2. DDPM/VP models

We choose the open-source DiT-XL/2(Peebles & Xie, 2023) model trained on ImageNet 256×256 as the search model to carry out the experiments. We compare the performance of the searched solver with DPM-Solver++ and UniPC on

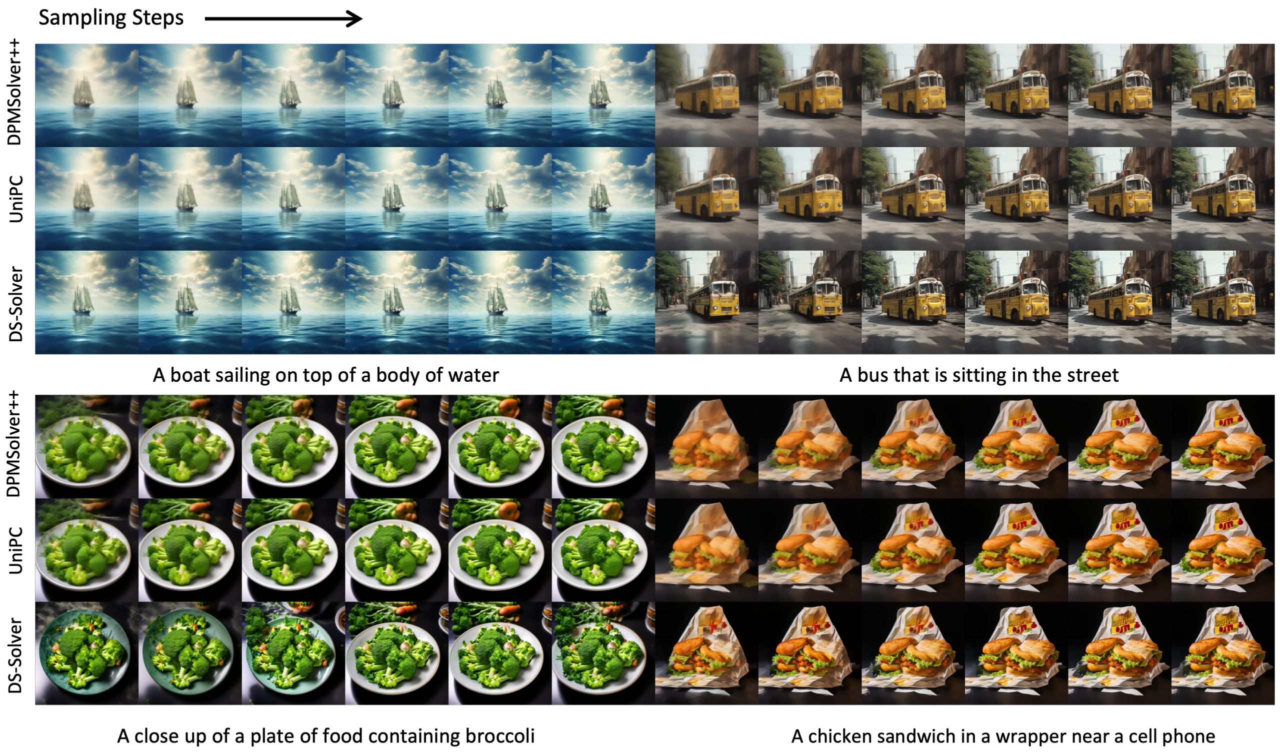
Sampling Steps
DPMSolver++
UniPC
DS-Solver
A boat sailing on top of a body of water
A bus that is sitting in the street
DPMSolver++
UniPC
DS-Solver
A close up of a plate of food containing broccoli
A chicken sandwich in a wrapper near a cell phone

Figure 5: The images generated from PixArt-Σ with CFG=2.0 equipped with Our DS-Solver (searched on DiT-XL/2-R256).In comparison to DPM-Solver++ and UniPC, our results consistently exhibit greater clarity and possess more details. Our solver achieves better quality from 5 to 10 steps(NFE).

Methods \NFEs	5	6	7	8	9	10
DPM-Solver++ with uniform-λ (Lu et al., 2023)	38.04	20.96	14.69	11.09	8.32	6.47
DPM-Solver++ with uniform-t (Lu et al., 2023)	31.32	14.36	7.62	4.93	3.77	3.23
DPM-Solver++ with uniform-λ-opt (Xue et al., 2024)	12.53	5.44	3.58	7.54	5.97	4.12
DPM-Solver++ with uniform-t-opt (Xue et al., 2024)	12.53	5.44	3.89	3.81	3.13	2.79
UniPC with uniform-λ (Zhao et al., 2023)	41.89	30.51	19.72	12.94	8.49	6.13
UniPC with uniform-t (Zhao et al., 2023)	23.48	10.31	5.73	4.06	3.39	3.04
UniPC with uniform-λ-opt (Xue et al., 2024)	8.66	4.46	3.57	3.72	3.40	3.01
UniPC with uniform-t-opt (Xue et al., 2024)	8.66	4.46	3.74	3.29	3.01	2.74
Searched-Solver	**7.40**	**3.94**	**2.79**	**2.51**	**2.37**	**2.33**

Table 2: **FID (↓) of different NFEs on DiT-XL/2-R256** . *-opt* indicates online optimization of the timesteps scheduler.

Methods \NFEs	5	6	7	8	9	10
UniPC with uniform-λ (Zhao et al., 2023)	41.14	19.81	13.01	9.83	8.31	7.01
UniPC with uniform-t (Zhao et al., 2023)	20.28	10.47	6.57	5.13	4.46	4.14
UniPC with uniform-λ-opt (Xue et al., 2024)	11.40	**5.95**	4.82	4.68	6.93	6.01
UniPC with uniform-t-opt (Xue et al., 2024)	11.40	**5.95**	4.64	4.36	4.05	3.81
Searched-solver(searched on DiT-XL/2-R256)	**10.28**	6.02	**4.31**	**3.74**	**3.54**	**3.64**

Table 3: **FID (↓) of different NFEs on DiT-XL/2-R512.** *-opt* indicates online optimization of the timesteps scheduler.

ImageNet 256×256 and ImageNet 512×512.

ImageNet 256×256**.** Following (Peebles & Xie, 2023) and (Xue et al., 2024), We arm pre-trained DiT-XL/2 with

Solver	Steps	CFG	GenEval Metrics			Overall
			Color.Attr	Two.Obj	Pos	
DPM++	5	2.0	6.50	33.08	4.75	0.40519
	8	2.0	5.25	39.65	5.75	0.43074
UniPC	5	2.0	6.50	34.85	5.25	0.41387
	8	2.0	6.72	40.66	6.00	0.44134
Ours	5	2.0	5.25	37.37	4.75	0.41933
	8	2.0	7.25	42.68	7.50	0.45064

Table 4: **Results on GenEval Benchmark for PixArt at 512 Resolution.** Our searched solver achieves better performance compared with UniPC/DPM++ on PixArt-512×512.

	Steps	FID	sFID	IS	PR	Recall
DPM++	5	60.0	209	25.59	0.36	0.20
DPM++	8	38.4	116.9	33.0	0.50	0.36
DPM++	10	35.6	114.7	33.7	0.53	0.37
UniPC	5	57.9	206.4	25.88	0.38	0.20
UniPC	8	37.6	115.3	33.3	0.51	0.36
UniPC	10	35.3	113.3	33.6	0.54	0.36
Ours	5	46.4	204	28.0	0.46	0.23
Ours	8	33.6	115.2	32.6	0.54	0.39
Ours	10	33.4	114.7	32.5	0.55	0.39

Table 5: Metrics of different NFEs on PixArt-α (Our Solver are searched on ImageNet 256x256).

CFG of 1.5 and apply CFG only on the first three channels. As shown in Table 2, our searched solver improves FID performance significantly and achieves 2.33 FID under 10 steps.

ImageNet 512×512**.** We directly apply the solver searched on 256×256 resolution to ImageNet 512×512. The result is also great to some extent, DiT-XL/2(512×512) achieves 3.64 FID under 10 steps, outperforming DPM-Solver++ and UniPC with a large gap.

Text to Image. As we search solver with DiT and its corresponding noise scheduler, so it is infeasible to apply our solver to other DDPM models with different β_{min} and β_{max}. Fortunately, we find (Chen et al., 2024b) and (Chen et al., 2023) also employ the same β_{min} and β_{max} as DiT. So we can provide the visualization results of our searched solver on PixArt-Σ and PixArt-α. Our visualization result is produced with CFG of 2. We take PixArt-alpha as the text-to-image model. We follow the evaluation pipeline of ADM and take COCO17-Val as the reference batch. We generate 5k images using DPM-Solver++, UniPC and our solver searched on DiT-XL/2-R256. Also, we provided the performance results on GenEval Benchmark (Ghosh et al., 2023) in Section 7.2.

7.3. Visualization of solver parameters

Searched Coefficients are visualized in Figure 1. The absolute value of searched coefficients corresponding to DDPM/VP shares a different pattern, coefficients in DDPM/VP are more concentrated on the diagonal while rectified-flow demonstrates a more flattened distribution. This indicates that there exists a more curved sampling path in DDPM/VP compared to rectified-flow.

Searched Timesteps are visualized in Figure 1. Compared to DDPM/VP, rectified-flow models focus more on the more noisy region, exhibiting small time deltas at the beginning. We fit the searched timestep of different NFE with polynomials and provide the respacing curves as follows:

$$\text{ReFlow} : -1.96t^4 + 3.51t^3 - 0.97t^2 + 0.43t, \quad (20)$$

$$\text{DDPM/VP} : -2.73t^4 + 6.30t^3 - 4.744t^2 + 2.17t, \quad (21)$$

$t \in [0, 1]$, and $t = 0$ indicates the most noisy timestep.

8. Conclusion

We have found a compact solver search space and proposed a novel differentiable solver search algorithm to identify the optimal solver. Our searched solver outperforms traditional solvers by a significant margin. Equipped with the searched solver, DDPM/VP and Rectified Flow models significantly improve under limited sampling steps. However, our proposed solver still has several limitations which we plan to address in future work.

9. Limitations

We have demonstrated text-to-image visualization with a small CFG value. However, it is intuitive that using a larger CFG would result in superior image quality. We attribute the inferior performance of large CFGs in our solver to the limitations of current naive solver structures and searching techniques. We hypothesize that incorporating predictor-corrector solver structures would enhance numerical stability and yield better images. Additionally, training with CFGs may also be beneficial.

Impact Statement

This paper proposes a search-based solver for fast diffusion sampling. We acknowledge that it could lower the barrier for creating diffusion-based AIGC contents.

Acknowledgments. This work is supported by the National Key R&D Program of China (No. 2022ZD0160900), Jiangsu Frontier Technology Research and Development Program (No. BF2024076), and the Collaborative Innovation Center of Novel Software Technology and Industrialization, Alibaba Group through the Alibaba Innovative Research Program.

References

Anderson, B. D. Reverse-time diffusion equation models. *Stochastic Processes and their Applications*, 12(3):313–326, 1982.

Bashforth, F. and Adams, J. C. *An attempt to test the theories of capillary action by comparing the theoretical and measured forms of drops of fluid*. University Press, 1883.

Brock, A., Donahue, J., and Simonyan, K. Large scale gan training for high fidelity natural image synthesis. *arXiv preprint arXiv:1809.11096*, 2018.

Chang, H., Zhang, H., Jiang, L., Liu, C., and Freeman, W. T. Maskgit: Masked generative image transformer. In *Proceedings of the IEEE/CVF Conference on Computer Vision and Pattern Recognition*, pp. 11315–11325, 2022.

Chen, D., Zhou, Z., Wang, C., Shen, C., and Lyu, S. On the trajectory regularity of ode-based diffusion sampling. *arXiv preprint arXiv:2405.11326*, 2024a.

Chen, J., Yu, J., Ge, C., Yao, L., Xie, E., Wu, Y., Wang, Z., Kwok, J., Luo, P., Lu, H., et al. Pixart-\alpha: Fast training of diffusion transformer for photorealistic text-to-image synthesis. *arXiv preprint arXiv:2310.00426*, 2023.

Chen, J., Ge, C., Xie, E., Wu, Y., Yao, L., Ren, X., Wang, Z., Luo, P., Lu, H., and Li, Z. Pixart-\sigma: Weak-to-strong training of diffusion transformer for 4k text-to-image generation. *arXiv preprint arXiv:2403.04692*, 2024b.

Chen, X., Liang, C., Huang, D., Real, E., Wang, K., Pham, H., Dong, X., Luong, T., Hsieh, C.-J., Lu, Y., et al. Symbolic discovery of optimization algorithms. *Advances in neural information processing systems*, 36, 2024c.

Esser, P., Kulal, S., Blattmann, A., Entezari, R., Müller, J., Saini, H., Levi, Y., Lorenz, D., Sauer, A., Boesel, F., et al. Scaling rectified flow transformers for high-resolution image synthesis. *arXiv preprint arXiv:2403.03206*, 2024.

Gao, Y., Pan, Z., Zhou, X., Kang, L., and Chaudhari, P. Fast diffusion probabilistic model sampling through the lens of backward error analysis. *arXiv preprint arXiv:2304.11446*, 2023.

Ghosh, D., Hajishirzi, H., and Schmidt, L. Geneval: An object-focused framework for evaluating text-to-image alignment. *Advances in Neural Information Processing Systems*, 36:52132–52152, 2023.

Ho, J., Jain, A., and Abbeel, P. Denoising diffusion probabilistic models. *Advances in neural information processing systems*, 33:6840–6851, 2020.

Kang, M., Zhang, R., Barnes, C., Paris, S., Kwak, S., Park, J., Shechtman, E., Zhu, J.-Y., and Park, T. Distilling diffusion models into conditional gans. *arXiv preprint arXiv:2405.05967*, 2024.

Karras, T., Aittala, M., Aila, T., and Laine, S. Elucidating the design space of diffusion-based generative models. *Advances in Neural Information Processing Systems*, 35:26565–26577, 2022.

Kim, D., Lai, C.-H., Liao, W.-H., Murata, N., Takida, Y., Uesaka, T., He, Y., Mitsufuji, Y., and Ermon, S. Consistency trajectory models: Learning probability flow ode trajectory of diffusion. *arXiv preprint arXiv:2310.02279*, 2023.

Lin, S., Wang, A., and Yang, X. Sdxl-lightning: Progressive adversarial diffusion distillation. *arXiv preprint arXiv:2402.13929*, 2024.

Lipman, Y., Chen, R. T., Ben-Hamu, H., Nickel, M., and Le, M. Flow matching for generative modeling. *arXiv preprint arXiv:2210.02747*, 2022.

Liu, X., Gong, C., and Liu, Q. Flow straight and fast: Learning to generate and transfer data with rectified flow. *arXiv preprint arXiv:2209.03003*, 2022.

Lu, C., Zhou, Y., Bao, F., Chen, J., LI, C., and Zhu, J. Dpm-solver: A fast ode solver for diffusion probabilistic model sampling in around 10 steps. In Koyejo, S., Mohamed, S., Agarwal, A., Belgrave, D., Cho, K., and Oh, A. (eds.), *Advances in Neural Information Processing Systems*, volume 35, pp. 5775–5787, 2022.

Lu, C., Zhou, Y., Bao, F., Chen, J., Li, C., and Zhu, J. Dpm-solver++: Fast solver for guided sampling of diffusion probabilistic models, 2023.

Ma, N., Goldstein, M., Albergo, M. S., Boffi, N. M., Vanden-Eijnden, E., and Xie, S. Sit: Exploring flow and diffusion-based generative models with scalable interpolant transformers. *arXiv preprint arXiv:2401.08740*, 2024.

Peebles, W. and Xie, S. Scalable diffusion models with transformers. In *Proceedings of the IEEE/CVF International Conference on Computer Vision*, pp. 4195–4205, 2023.

Sabour, A., Fidler, S., and Kreis, K. Align your steps: Optimizing sampling schedules in diffusion models. *arXiv preprint arXiv:2404.14507*, 2024.

Salimans, T. and Ho, J. Progressive distillation for fast sampling of diffusion models. *arXiv preprint arXiv:2202.00512*, 2022.

Sauer, A., Schwarz, K., and Geiger, A. Stylegan-xl: Scaling stylegan to large diverse datasets. In *ACM SIGGRAPH 2022 conference proceedings*, pp. 1–10, 2022.

Shaul, N., Perez, J., Chen, R. T., Thabet, A., Pumarola, A., and Lipman, Y. Bespoke solvers for generative flow models. *arXiv preprint arXiv:2310.19075*, 2023.

Song, J., Meng, C., and Ermon, S. Denoising diffusion implicit models. *arXiv:2010.02502*, October 2020a. URL `https://arxiv.org/abs/2010.02502`.

Song, T., Feng, W., Wang, S., Li, X., Ge, T., Zheng, B., and Wang, L. Dmm: Building a versatile image generation model via distillation-based model merging. *arXiv preprint arXiv:2504.12364*, 2025.

Song, Y., Sohl-Dickstein, J., Kingma, D. P., Kumar, A., Ermon, S., and Poole, B. Score-based generative modeling through stochastic differential equations. *arXiv preprint arXiv:2011.13456*, 2020b.

Song, Y., Dhariwal, P., Chen, M., and Sutskever, I. Consistency models. *arXiv preprint arXiv:2303.01469*, 2023.

Wang, F.-Y., Huang, Z., Bergman, A. W., Shen, D., Gao, P., Lingelbach, M., Sun, K., Bian, W., Song, G., Liu, Y., et al. Phased consistency model. *arXiv preprint arXiv:2405.18407*, 2024a.

Wang, S., Teng, Y., and Wang, L. Deep equilibrium object detection. In *Proceedings of the IEEE/CVF International Conference on Computer Vision*, pp. 6296–6306, 2023.

Wang, S., Li, Z., Song, T., Li, X., Ge, T., Zheng, B., and Wang, L. Flowdcn: Exploring dcn-like architectures for fast image generation with arbitrary resolution. *arXiv preprint arXiv:2410.22655*, 2024b.

Wang, S., Tian, Z., Huang, W., and Wang, L. Ddt: Decoupled diffusion transformer. *arXiv preprint arXiv:2504.05741*, 2025.

Xu, C., Song, T., Feng, W., Li, X., Ge, T., Zheng, B., and Wang, L. Accelerating image generation with sub-path linear approximation model. In *ECCV*, pp. 323–339, 2024.

Xue, S., Liu, Z., Chen, F., Zhang, S., Hu, T., Xie, E., and Li, Z. Accelerating diffusion sampling with optimized time steps. In *Proceedings of the IEEE/CVF Conference on Computer Vision and Pattern Recognition*, pp. 8292–8301, 2024.

Yin, T., Gharbi, M., Zhang, R., Shechtman, E., Durand, F., Freeman, W. T., and Park, T. One-step diffusion with distribution matching distillation. In *Proceedings of the IEEE/CVF Conference on Computer Vision and Pattern Recognition*, pp. 6613–6623, 2024.

Zhang, Q. and Chen, Y. Fast sampling of diffusion models with exponential integrator. In *The Eleventh International Conference on Learning Representations*, 2023.

Zhao, W., Bai, L., Rao, Y., Zhou, J., and Lu, J. Unipc: A unified predictor-corrector framework for fast sampling of diffusion models. *arXiv preprint arXiv:2302.04867*, 2023.

Zhao, W., Shi, M., Yu, X., Zhou, J., and Lu, J. Flowturbo: Towards real-time flow-based image generation with velocity refiner. *arXiv preprint arXiv:2409.18128*, 2024.

Zheng, J., Hu, M., Fan, Z., Wang, C., Ding, C., Tao, D., and Cham, T.-J. Trajectory consistency distillation. *arXiv preprint arXiv:2402.19159*, 2024.

Zhou, M., Zheng, H., Wang, Z., Yin, M., and Huang, H. Score identity distillation: Exponentially fast distillation of pretrained diffusion models for one-step generation. In *Forty-first International Conference on Machine Learning*, 2024.

A. More Metrics of Searched Solver

We adhere to the evaluation guidelines provided by ADM and DM-nonuniform, reporting only the FID as the standard metric in Figure 4a. To clarify, we do not report selective results on rectified flow models; we present sFID, IS, PR, and Recall metrics for SiT-XL(R256), FlowDCN-XL/2(R256), and FlowDCN-B/2(R256). Our solver searched on FlowDCN-B/2, consistently outperforms the handcrafted solvers across FID, sFID, IS, and Recall metrics.

B. Computational complexity compared to other methods.

For sampling. When performing sampling over n time steps, our solver caches all pre-sampled predictions, resulting in a memory complexity of $\mathcal{O}(n)$. The model function evaluation also has a complexity of $\mathcal{O}(n)$ ($\mathcal{O}(2 \times n)$ for CFG enabled). It is important to note that the memory required for caching predictions is negligible compared to that used by model weights and activations. Besides classic methods, we have also included a comparison with the latest Flowturbo published on NeurIPS24.

	Steps	NFE	NFE-CFG	Cache Pred	Order	search samples
Adam2	n	n	2n	2	2	/
Adam4	n	n	2n	4	4	/
heun	n	2n	4n	2	2	/
DPM-Solver++	n	n	2n	2	2	/
UniPC	n	n	2n	3	3	/
FlowTurbo	n	>n	>2n	2	2	540000(Real)
our	n	n	2n	n	n	50000(Generated)

For searching. Solver-based algorithms, limited by their searchable parameter sizes, demonstrate significantly lower performance in few-step settings compared to distillation-based algorithms(5/6steps), making direct comparisons inappropriate. Consequently, we selected algorithms that are both acceleratable on ImageNet and comparable in performance, including popular methods such as DPM-Solver++, UniPC, and classic Adams-like linear multi-step methods. Since our experiments primarily utilize SiT, DiT, and FlowDCN that trained on the ImageNet dataset. We also provide fair comparisons by incorporating the latest acceleration method, FlowTurbo. Additionally, we have included results from the heun method as reported in FlowTurbo.

C. Ablation on Search Samples

We ablate the number of search samples on the 10-step and 8-step solver settings. *Samples* means the total training samples the searched solver has seen. *Unique Samples* means the total distinct samples the searched solver has seen. Our searched solver converges fast and gets saturated near 30000 samples.

iters(10-step-solver)	samples	unique samples	FID	IS	PR	Recall
313	10000	10000	2.54	239	0.79	0.59
626	20000	10000	2.38	239	0.79	0.60
939	30000	10000	2.49	240	0.79	0.59
1252	40000	10000	2.29	239	0.80	0.60
1565	50000	10000	2.41	240	0.80	0.59
626	20000	20000	2.47	237	0.78	0.60
939	30000	30000	2.40	238	0.79	0.60
1252	40000	40000	2.48	237	0.80	0.59
1565	50000	50000	2.41	239	0.80	0.59

D. Solver Across different variance schedules

Since our solvers are searched on a specific noise scheduler and its corresponding pre-trained models, applying the searched coefficients and timesteps to other noise schedulers yields meaningless results. We have tried applied searched solver on SiT(Rectified flow) and DiT(DDPM with $\beta_{min} = 0.1, \beta_{max} = 20$) to SD1.5(DDPM with $\beta_{min} = 0.085, \beta_{max} = 12$), but the results were inconclusive. Notably, despite sharing the DDPM name, DiT and SD1.5 employ distinct β_{min}, β_{max} values, thereby featuring different noise schedulers. A more in-depth discussion of these experiments can be found in Section(Extend to DDPM/VP).

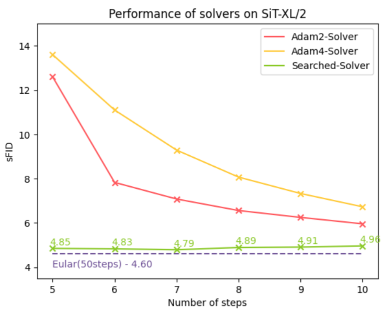

(a) SiT-XL/2-R256

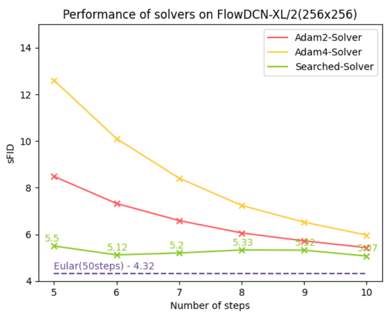

(b) FlowDCN-XL/2-R256

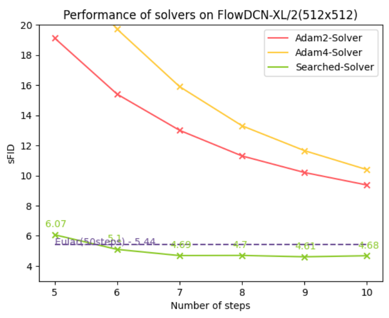

(c) FlowDCN-XL/2-R512

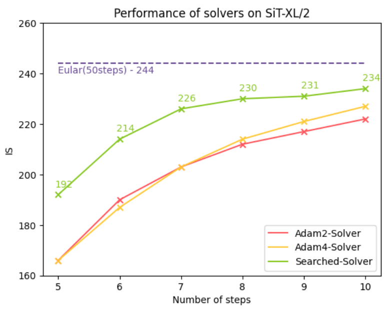

(d) SiT-XL/2-R256

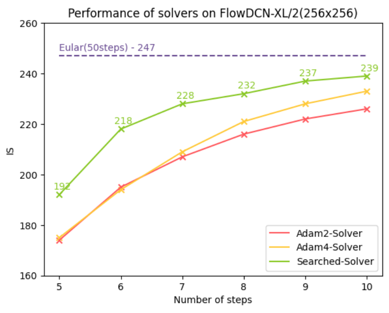

(e) FlowDCN-XL/2-R256

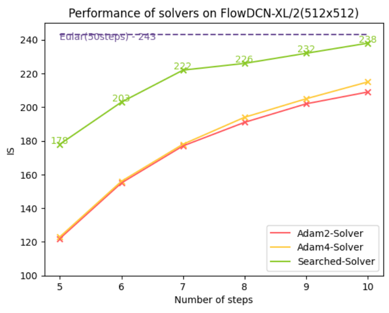

(f) FlowDCN-XL/2-R512

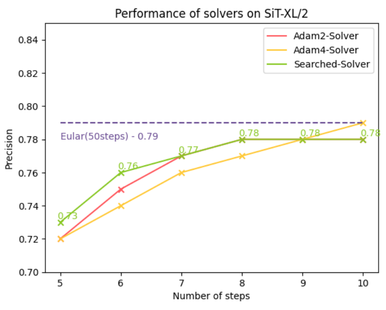

(g) SiT-XL/2-R256

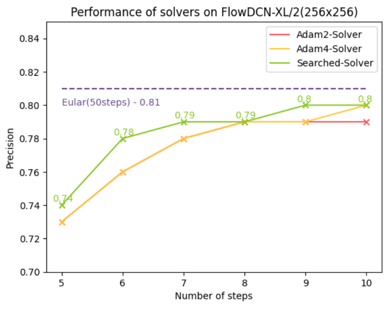

(h) FlowDCN-XL/2-R256

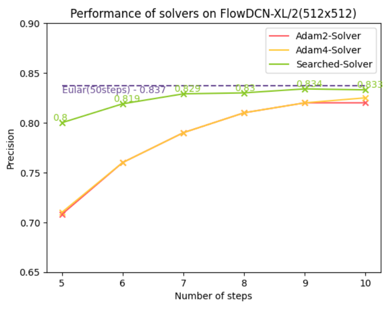

(i) FlowDCN-XL/2-R512

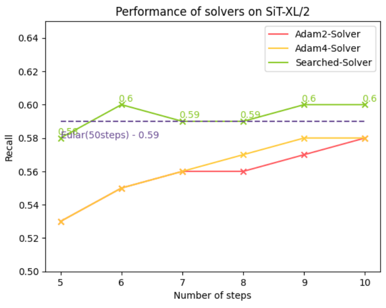

(j) SiT-XL/2-R256

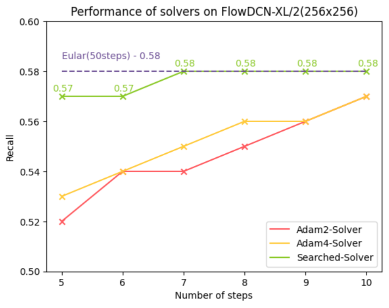

(k) FlowDCN-XL/2-R256

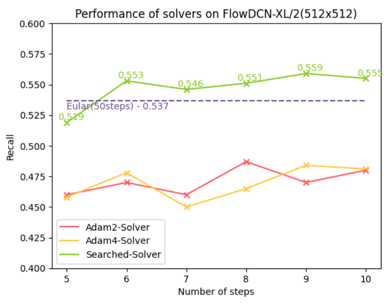

(l) FlowDCN-XL/2-R512

Figure 6: **The same searched solver on different Rectified-Flow Models.** R256 and R512 indicate the generation resolution of given model. We search solver with FlowDCN-B/2 on ImageNet-256×256 and evaluate it with SiT-XL/2 and FlowDCN-XL/2 on different resolution datasets. Our searched solver outperforms traditional solvers by a significant margin.

iters(8-step-solver)	samples	unique samples	FID	IS	PR	Recall
313	10000	10000	2.99	228	0.78	0.59
626	20000	10000	2.78	229	0.79	0.60
939	30000	10000	2.72	235	0.79	0.60
1252	40000	10000	2.67	228	0.79	0.60
1565	50000	10000	2.69	235	0.79	0.59
626	20000	20000	2.70	231	0.79	0.59
939	30000	30000	2.82	232	0.79	0.59
1252	40000	40000	2.79	231	0.79	0.60
1565	50000	50000	2.65	234	0.79	0.60

E. Solver for different variance schedules

As every DDPM has a corresponding continuous VP scheduler, so we can transform the discreet DDPM into continuous VP, thus we successfully searched better solver compared to DPM-Solvers. The details can be found in Section 6. To put it simply, under the empowerment of our high-order solver, the performance of DDPM and FM does not differ significantly (8, 9, 10 steps), which contradicts the common belief that FM is stronger at limited sampling steps.

F. Text to image Distillation Experiments

We unify distillation and solver search to obtain high-quality multi-step generative models. We adopt adversarial training and trajectory supervision. We will open source the training code of unified training techniques.

Table 6: Performance comparison on validation set of COCO-2017.

Method	Res.	Time (↓)	# Steps	# Param.	FID (↓)
SDv1-5+DPMSolver (Upper-Bound) (Lu et al., 2022)	512	0.88s	25	0.9B	20.1
Rectified Flow	512	0.88s	25	0.9B	21.65
Rectified Diffusion	512	0.88s	25	0.9B	21.28
Rectified Flow	512	0.21s	4	0.9B	103.48
PeRFlow	512	0.21s	4	0.9B	22.97
Rectified Diffusion	512	0.21s	4	0.9B	20.64
Ours(Distillation+solver search)	512	0.21s	4	0.9B	18.99
PeRFlow-SDXL	1024	0.71s	4	3B	27.06
Rectified Diffusion-SDXL	1024	0.71s	4	3B	25.81
Ours(LORA+Distillation+solver search)	1024	0.71s	4	3B	21.3

Table 7: Performance comparison on COCO-2014.

Method	Res.	Time (↓)	# Steps	# Param.	FID (↓)
Stable Diffusion XL (3B) and its accelerated or distilled versions					
SDXL-Turbo	512	0.34s	4	3B	23.19
SDXL-Lightning	1024	0.71s	4	3B	24.56
DMDv2	1024	0.71s	4	3B	19.32
LCM	1024	0.71s	4	3B	22.16
Phased Consistency Model	1024	0.71s	4	3B	21.04
PeRFlow-XL	1024	0.71s	4	3B	20.99
Rectified Diffusion-XL (Phased)	1024	0.71s	4	3B	19.71
Ours(LORA+Distillation+solver search)	1024	0.71s	4	3B	11.4

G. Limitations.

We place the limitation at the appendix, in order to provide more discussion space and obtain more insights from reviews. We copy the original limitation content and add more.

Misalignd Reconstrucion loss and Performance. Our proposed methods are specifically designed to minimize integral error within a limited number of steps. However, ablation studies reveal a mismatch between FID performance and Reconstruction error. To address this issue, we plan to enhance our searched solver by incorporating distribution matching supervision, thereby better aligning sampling quality.

Larger CFG Inference. In the main paper, we demonstrate text-to-image visualization with a small CFG value. However, it is intuitive that utilizing a larger CFG would result in superior image quality. We attribute the inferior performance of large CFGs on our solver to the limitations of current naive solver structures and searching techniques. We hypothesize that incorporating predictor-corrector solver structures would enhance numerical stability and yield better images. Additionally, training with CFGs may also be beneficial.

Resource Consumption We can hard code the searched coefficients and timesteps into the program files. However, Compared to hand-crafted solvers, our solver still needs a searching process.

H. Proof of pre-integral error expectation

Theorem H.1. *Given sampling time interval* $[t_i, t_{i+1}]$ *and suppose* $\mathcal{C}_j(\boldsymbol{x}) = g_j(\boldsymbol{x}) + b_i^j$, *Adams-like linear multi-step methods will introduce an upper error bound of* $(t_{i+1} - t_i)\mathbb{E}_{\boldsymbol{x}_i}||\sum_{j=0}^{i} \boldsymbol{v}_j g_j(\boldsymbol{x}_i)||$.

Our solver search(replacing $\mathcal{C}_j(\boldsymbol{x})$ *with* $\mathbb{E}_{\boldsymbol{x}_i}[\mathcal{C}_j(\boldsymbol{x}_i)]$*) owns an upper error bound of* $(t_{i+1} - t_i)\mathbb{E}_{\boldsymbol{x}_i}||\sum_{j=0}^{i} \boldsymbol{v}_j[g_j(\boldsymbol{x}_i) - \mathbb{E}_{\boldsymbol{x}_i} g_j(\boldsymbol{x}_i)||$

Proof. Suppose $\mathcal{C}_j(\boldsymbol{x}_i) = g_j(\boldsymbol{x}_i) + b_i^j$. Adams-like linear multi-step methods would not consider x-related interpolation. thus pre-integral coefficients of Adams-like linear multi-step methods will only reduce into b.

We obtain the error expectation of the pre-integral of Adams-like linear multi-step methods:

$$\mathbb{E}_{\boldsymbol{x}_i}||\sum_{j=0}^{i} \boldsymbol{v}_j[\mathcal{C}_j(\boldsymbol{x}_i)](t_{i+1} - t_i) - \sum_{j=0}^{i} \boldsymbol{v}_j b_i^j (t_{i+1} - t_i)|| \tag{22}$$

$$= \mathbb{E}_{\boldsymbol{x}_i}||\sum_{j=0}^{i} \boldsymbol{v}_j (t_{i+1} - t_i)[\mathcal{C}_j(\boldsymbol{x}_i) - b_i^j|| \tag{23}$$

$$= (t_{i+1} - t_i)\mathbb{E}_{\boldsymbol{x}_i}||\sum_{j=0}^{i} \boldsymbol{v}_j g_j(\boldsymbol{x}_i)|| \tag{24}$$

We obtain the error expectation of the pre-integral of our solver search methods:

$$\mathbb{E}_{\boldsymbol{x}_i}||\sum_{j=0}^{i} \boldsymbol{v}_j[\mathcal{C}_j(\boldsymbol{x}_i)](t_{i+1} - t_i) - \sum_{j=0}^{i} \boldsymbol{v}_j \mathbb{E}_{\boldsymbol{x}_i}[\mathcal{C}_j(\boldsymbol{x}_i)](t_{i+1} - t_i)|| \tag{25}$$

$$= \mathbb{E}_{\boldsymbol{x}_i}||\sum_{j=0}^{i} \boldsymbol{v}_j (t_{i+1} - t_i)[\mathcal{C}_j(\boldsymbol{x}_i) - \mathbb{E}_{\boldsymbol{x}_i}\mathcal{C}_j(\boldsymbol{x}_i)|| \tag{26}$$

$$= (t_{i+1} - t_i)\mathbb{E}_{\boldsymbol{x}_i}||\sum_{j=0}^{i} \boldsymbol{v}_j[g_j(\boldsymbol{x}_i) - \mathbb{E}_{\boldsymbol{x}_i} g_j(\boldsymbol{x}_i)|| \tag{27}$$

Next, define the optimization problem:

$$E = \mathbb{E}_{\boldsymbol{x}_i}||\sum_{j=0}^{i} \boldsymbol{v}_j[g_j(\boldsymbol{x}_i) - a_j]||_2^2.$$

We suppose different v_j are orthogonal and $||v_j||_2^2 = 1$. As we leave c_j^i as the expectation of $\mathcal{C}_j(\boldsymbol{x}_i)$, we will demonstrate this choice is optimal.

$$\frac{\partial E}{\partial a_j} = -2\mathbb{E}_{\boldsymbol{x}_i}(||v_j||_2^2(g_j(x_i) - a_j)) \tag{28}$$

Let $\frac{\partial E}{\partial a_j} = 0$, we obtain: $a_j = \frac{\mathbb{E}_{\boldsymbol{x}_i} g_i(x_i)||v_j||_2^2}{\mathbb{E}_{\boldsymbol{x}_i}||v_j||_2^2} = \mathbb{E}_{\boldsymbol{x}_i} g_j(\boldsymbol{x}_i) = \mathbb{E}_{\boldsymbol{x}_i}\mathcal{C}_j(\boldsymbol{x}_i) - b_i^j$.

So our searched solver has a lower and optimal error expectation:

$$(t_{i+1} - t_i)\mathbb{E}_{\boldsymbol{x}_i}||\sum_{j=0}^{i} \boldsymbol{v}_j[g_j(\boldsymbol{x}_i) - \mathbb{E}_{\boldsymbol{x}_i} g_j(\boldsymbol{x}_i)]|| \leq (t_{i+1} - t_i)\mathbb{E}_{\boldsymbol{x}_i}||\sum_{j=0}^{i} \boldsymbol{v}_j g_j(\boldsymbol{x}_i)|| \tag{29}$$

Recall Assumption 4.1, the integral upper error bound of universal interpolation $\mathcal{P}$ will be:

$$
\begin{aligned}
&||\int_{t_i}^{t_{i+1}} v(\boldsymbol{x}_t,t)dt - \sum_{j=0}^{i}\boldsymbol{v}_j\int_{t_i}^{t_{i+1}}\mathcal{P}(\boldsymbol{x}_t,t,\boldsymbol{x}_j,t_j)dt||. && (30)\\
=&||\int_{t_i}^{t_{i+1}} v(\boldsymbol{x}_t,t)dt - \int_{t_i}^{t_{i+1}}\sum_{j=0}^{i}\mathcal{P}(\boldsymbol{x}_t,t,\boldsymbol{x}_j,t_j)\boldsymbol{v}_j dt||. && (31)\\
=&||\int_{t_i}^{t_{i+1}} [v(\boldsymbol{x}_t,t) - \sum_{j=0}^{i}\mathcal{P}(\boldsymbol{x}_t,t,\boldsymbol{x}_j,t_j)\boldsymbol{v}_j]dt||. && (32)\\
<&\int_{t_i}^{t_{i+1}} ||v(\boldsymbol{x}_t,t) - \sum_{j=0}^{i}\mathcal{P}(\boldsymbol{x}_t,t,\boldsymbol{x}_j,t_j)\boldsymbol{v}_j||dt. && (33)\\
<&(t_{i+1}-t_i)[\mathcal{O}(d\boldsymbol{x}^m)+\mathcal{O}(dt^n)] && (34)
\end{aligned}
$$

Combining Equation (34) and the error expectation of the pre-integral part, we will get the total error bound of the solver search.

$$
\begin{aligned}
&||\int_{t_i}^{t_{i+1}} v(\boldsymbol{x}_t,t)dt - \sum_{j=0}^{i}\boldsymbol{v}_j\mathbb{E}_{\boldsymbol{x}_i}[\mathcal{C}_j(\boldsymbol{x}_i)](t_{i+1}-t_i)||. && (35)\\
=&||\int_{t_i}^{t_{i+1}} v(\boldsymbol{x}_t,t)dt - \sum_{j=0}^{i}\boldsymbol{v}_j\int_{t_i}^{t_{i+1}}\mathcal{P}(\boldsymbol{x}_t,t,\boldsymbol{x}_j,t_j)dt + && (36)\\
&\sum_{j=0}^{i}\boldsymbol{v}_j\int_{t_i}^{t_{i+1}}\mathcal{P}(\boldsymbol{x}_t,t,\boldsymbol{x}_j,t_j)dt - \sum_{j=0}^{i}\boldsymbol{v}_j\mathbb{E}_{\boldsymbol{x}_i}[\mathcal{C}_j(\boldsymbol{x}_i)](t_{i+1}-t_i)||. && (37)\\
<&||\int_{t_i}^{t_{i+1}} v(\boldsymbol{x}_t,t)dt - \sum_{j=0}^{i}\boldsymbol{v}_j\int_{t_i}^{t_{i+1}}\mathcal{P}(\boldsymbol{x}_t,t,\boldsymbol{x}_j,t_j)dt|| + && (38)\\
&||\sum_{j=0}^{i}\boldsymbol{v}_j\int_{t_i}^{t_{i+1}}\mathcal{P}(\boldsymbol{x}_t,t,\boldsymbol{x}_j,t_j)dt - \sum_{j=0}^{i}\boldsymbol{v}_j\mathbb{E}_{\boldsymbol{x}_i}[\mathcal{C}_j(\boldsymbol{x}_i)](t_{i+1}-t_i)||. && (39)\\
=&||\int_{t_i}^{t_{i+1}} v(\boldsymbol{x}_t,t)dt - \sum_{j=0}^{i}\boldsymbol{v}_j\int_{t_i}^{t_{i+1}}\mathcal{P}(\boldsymbol{x}_t,t,\boldsymbol{x}_j,t_j)dt|| + && (40)\\
&||\sum_{j=0}^{i}\boldsymbol{v}_j[\mathcal{C}_j(\boldsymbol{x}_i)](t_{i+1}-t_i) - \sum_{j=0}^{i}\boldsymbol{v}_j\mathbb{E}_{\boldsymbol{x}_i}[\mathcal{C}_j(\boldsymbol{x}_i)](t_{i+1}-t_i)||. && (41)\\
<&(t_{i+1}-t_i)[\mathcal{O}(d\boldsymbol{x}^m)+\mathcal{O}(dt^n)] + (t_{i+1}-t_i)\mathbb{E}_{\boldsymbol{x}_i}||\sum_{j=0}^{i}\boldsymbol{v}_j[g_j(\boldsymbol{x}_i)-\mathbb{E}_{\boldsymbol{x}_i}g_j(\boldsymbol{x}_i)]|| && (42)\\
<&(t_{i+1}-t_i)([\mathcal{O}(d\boldsymbol{x}^m)+\mathcal{O}(dt^n)] + \mathbb{E}_{\boldsymbol{x}_i}||\sum_{j=0}^{i}\boldsymbol{v}_j[g_j(\boldsymbol{x}_i)-\mathbb{E}_{\boldsymbol{x}_i}g_j(\boldsymbol{x}_i)]||) && (43)
\end{aligned}
$$

Since $((\mathcal{O}(d\boldsymbol{x}^m)+\mathcal{O}(dt^n))$ is much smaller than $\mathbb{E}_{\boldsymbol{x}_i}||\sum_{j=0}^{i}\boldsymbol{v}_j[g_j(\boldsymbol{x}_i)-\mathbb{E}_{\boldsymbol{x}_i}g_j(\boldsymbol{x}_i)]||$. We can omit the $((\mathcal{O}(d\boldsymbol{x}^m)+\mathcal{O}(dt^n))$ term.

□

I. Proof of total upper error bound

Theorem I.1. *Compared to Adams-like linear multi-step methods. Our Solver search has a small upper error bound.*

The total upper error bound of Adams-like linear multi-step methods is:

$$
\sum_{i=0}^{N-1}(\frac{1}{N})\sum_{j=0}^{i}\eta|b_i^j| + \mathbb{E}_{\boldsymbol{x}_i}||\sum_{j=0}^{i}\boldsymbol{v}_j[g_j(\boldsymbol{x}_i)]||)
$$

The total upper error bound of Our solver search is:

$$\sum_{i=0}^{N-1}(t_{i+1}-t_i)\sum_{j=0}^{i}\eta|\mathbb{E}_{\boldsymbol{x}_i}g_j(\boldsymbol{x}_i)+b_i^j|+\mathbb{E}_{\boldsymbol{x}_i}||\sum_{j=0}^{i}\boldsymbol{v}_j g_j(\boldsymbol{x}_i)-\mathbb{E}_{\boldsymbol{x}_i}g_j(\boldsymbol{x}_i)||)$$

Proof. We donate the continuous integral result of the ideal velocity field $\hat{\boldsymbol{v}}$ as $\hat{\boldsymbol{x}}$, the solved integral result of the ideal velocity field $\hat{\boldsymbol{v}}$ as $\hat{\boldsymbol{x}}_N$, the continuous integral result of the pre-trained velocity model $\boldsymbol{v}_\theta$ as $\hat{\boldsymbol{x}}$, the solved integral result of the pre-trained velocity model $\boldsymbol{v}_\theta$ as $\boldsymbol{x}_N$.

$$\boldsymbol{x}_N=\boldsymbol{\epsilon}+\sum_{i=0}^{N-1}\sum_{j=0}^{i}\boldsymbol{v}_j c_i^j(t_{i+1}-t_i) \tag{44}$$

The error caused by the non-ideal velocity estimation model can be formulated in the following equation. we can employ triangular inequalities to obtain the error-bound $||\boldsymbol{x}_N-\hat{x}_N||$, which is related to solver coefficients and timestep choices.

$$\begin{aligned}||\boldsymbol{x}_N-\hat{\boldsymbol{x}}_N|| &= |\sum_{i=0}^{N-1}\sum_{j=0}^{i}(\boldsymbol{v}_j-\hat{\boldsymbol{v}}_j)c_i^j(t_{i+1}-t_i)|\\
&\le \sum_{i=0}^{N-1}\sum_{j=0}^{i}|(\boldsymbol{v}_j-\hat{\boldsymbol{v}}_j)c_i^j(t_{i+1}-t_i)|\\
&\le \sum_{i=0}^{N-1}\sum_{j=0}^{i}|\boldsymbol{v}_j-\hat{\boldsymbol{v}}_j)|\times|c_i^j(t_{i+1}-t_i)|\\
&\le \eta\sum_{i=0}^{N-1}\sum_{j=0}^{i}|c_i^j(t_{i+1}-t_i)|\end{aligned}$$

The total error of our searched solver is:

$$\begin{aligned}&||\boldsymbol{x}_N-\hat{\boldsymbol{x}}||\\
=&||\boldsymbol{x}_N-\hat{\boldsymbol{x}}_N+\hat{\boldsymbol{x}}_N-\hat{\boldsymbol{x}}||\\
\le&||\boldsymbol{x}_N-\hat{\boldsymbol{x}}_N||+||\hat{\boldsymbol{x}}_N-\hat{\boldsymbol{x}}||\\
\le&\eta\sum_{i=0}^{N-1}\sum_{j=0}^{i}|c_i^j(t_{i+1}-t_i)|+\\
&\sum_{i=0}^{N-1}(t_{i+1}-t_i)(\mathcal{O}(d\boldsymbol{x}^m)+\mathcal{O}(dt^n)+\mathbb{E}_{\boldsymbol{x}_i}||\sum_{j=0}^{i}\boldsymbol{v}_j[g_j(\boldsymbol{x}_i)-\mathbb{E}_{\boldsymbol{x}_i}g_j(\boldsymbol{x}_i)]||)\\
\approx&\sum_{i=0}^{N-1}\eta\sum_{j=0}^{i}|c_i^j(t_{i+1}-t_i)|+(t_{i+1}-t_i)\mathbb{E}_{\boldsymbol{x}_i}||\sum_{j=0}^{i}\boldsymbol{v}_j[g_j(\boldsymbol{x}_i)-\mathbb{E}_{\boldsymbol{x}_i}g_j(\boldsymbol{x}_i)]||)\\
=&\sum_{i=0}^{N-1}(t_{i+1}-t_i)\sum_{j=0}^{i}\eta|\mathbb{E}_{\boldsymbol{x}_i}g_j(\boldsymbol{x}_i)+b_i^j|+\mathbb{E}_{\boldsymbol{x}_i}||\sum_{j=0}^{i}\boldsymbol{v}_j[g_j(\boldsymbol{x}_i)-\mathbb{E}_{\boldsymbol{x}_i}g_j(\boldsymbol{x}_i)]||)\end{aligned}$$

The total error of Adams-like linear multi-step method is:

$$\sum_{i=0}^{N-1}(\frac{1}{N})\sum_{j=0}^{i}\eta|b_i^j|+\mathbb{E}_{\boldsymbol{x}_i}||\sum_{j=0}^{i}\boldsymbol{v}_j[g_j(\boldsymbol{x}_i)]||)$$

Obviously, as $(\sum_{j=0}^{i}\eta|b_i^j|+\mathbb{E}_{\boldsymbol{x}_i}||\sum_{j=0}^{i}\boldsymbol{v}_j[g_j(\boldsymbol{x}_i)]||)$ is not equal between different timestep intervals, Optimized timesteps owns smaller upper error bound than uniform timesteps.

Recall that $\eta\ll||v_j||$, the error is mainly determined by $\mathbb{E}_{\boldsymbol{x}_i}||\sum_{j=0}^{i}\boldsymbol{v}_j[g_j(\boldsymbol{x}_i)]||$.

Recall that $\mathbb{E}_{\boldsymbol{x}_i}||\sum_{j=0}^{i}\boldsymbol{v}_j[g_j(\boldsymbol{x}_i)-\mathbb{E}_{\boldsymbol{x}_i}g_j(\boldsymbol{x}_i)]||\le\mathbb{E}_{\boldsymbol{x}_i}||\sum_{j=0}^{i}\boldsymbol{v}_j[g_j(\boldsymbol{x}_i)]||$, thus our solver search has a minimal upper error bound because we search coefficients and timesteps simultaneously.

□

J. Searched Parameters

We provide the searched parameters Δt and c_i^j. Note c_i^j needs to be converted into $\mathcal{M}$ follwing Algorithm 1.

J.1. Solver Searched on SiT-XL/2

NFE	TimeDeltas Δt	Coeffcients c_i^j
5	$\begin{bmatrix} 0.0424 \\ 0.1225 \\ 0.2144 \\ 0.3073 \\ 0.3135 \end{bmatrix}$	$\begin{bmatrix} 0.0 & 0.0 & 0.0 & 0.0 & 0.0 \\ -1.17 & 0.0 & 0.0 & 0.0 & 0.0 \\ 1.07 & -1.83 & 0.0 & 0.0 & 0.0 \\ 0.0 & 0.0 & -0.93 & 0.0 & 0.0 \\ 0.0 & 0.0 & 0.0 & -0.71 & 0.0 \end{bmatrix}$
6	$\begin{bmatrix} 0.0389 \\ 0.0976 \\ 0.161 \\ 0.2046 \\ 0.2762 \\ 0.2217 \end{bmatrix}$	$\begin{bmatrix} 0.0 & 0.0 & 0.0 & 0.0 & 0.0 & 0.0 \\ -1.04 & 0.0 & 0.0 & 0.0 & 0.0 & 0.0 \\ 1.62 & -2.98 & 0.0 & 0.0 & 0.0 & 0.0 \\ -1.32 & 2.52 & -2.04 & 0.0 & 0.0 & 0.0 \\ 0.0 & 0.0 & 0.0 & -0.76 & 0.0 & 0.0 \\ 0.0 & 0.0 & 0.0 & 0.0 & -0.66 & 0.0 \end{bmatrix}$
7	$\begin{bmatrix} 0.0299 \\ 0.0735 \\ 0.1119 \\ 0.1451 \\ 0.1959 \\ 0.2698 \\ 0.1738 \end{bmatrix}$	$\begin{bmatrix} 0.0 & 0.0 & 0.0 & 0.0 & 0.0 & 0.0 & 0.0 \\ -0.93 & 0.0 & 0.0 & 0.0 & 0.0 & 0.0 & 0.0 \\ 1.23 & -2.31 & 0.0 & 0.0 & 0.0 & 0.0 & 0.0 \\ -0.59 & 1.53 & -2.09 & 0.0 & 0.0 & 0.0 & 0.0 \\ -0.09 & -0.07 & 0.99 & -1.91 & 0.0 & 0.0 & 0.0 \\ 0.05 & -0.21 & 0.09 & 0.55 & -1.47 & 0.0 & 0.0 \\ -0.05 & 0.19 & -0.31 & 0.37 & 0.67 & -1.79 & 0.0 \end{bmatrix}$
8	$\begin{bmatrix} 0.0303 \\ 0.0702 \\ 0.0716 \\ 0.1112 \\ 0.1501 \\ 0.1833 \\ 0.2475 \\ 0.1358 \end{bmatrix}$	$\begin{bmatrix} 0.0 & 0.0 & 0.0 & 0.0 & 0.0 & 0.0 & 0.0 & 0.0 \\ -0.92 & 0.0 & 0.0 & 0.0 & 0.0 & 0.0 & 0.0 & 0.0 \\ 0.78 & -1.7 & 0.0 & 0.0 & 0.0 & 0.0 & 0.0 & 0.0 \\ 0.06 & 0.52 & -1.76 & 0.0 & 0.0 & 0.0 & 0.0 & 0.0 \\ -0.02 & -0.16 & 0.98 & -1.8 & 0.0 & 0.0 & 0.0 & 0.0 \\ -0.02 & -0.12 & 0.22 & 0.24 & -1.36 & 0.0 & 0.0 & 0.0 \\ -0.1 & 0.06 & -0.02 & 0.18 & 0.12 & -1.1 & 0.0 & 0.0 \\ -0.16 & 0.14 & -0.02 & -0.02 & 0.38 & 0.32 & -1.72 & 0.0 \end{bmatrix}$
9	$\begin{bmatrix} 0.028 \\ 0.0624 \\ 0.0717 \\ 0.0894 \\ 0.1092 \\ 0.1307 \\ 0.1729 \\ 0.2198 \\ 0.1159 \end{bmatrix}$	$\begin{bmatrix} 0.0 & 0.0 & 0.0 & 0.0 & 0.0 & 0.0 & 0.0 & 0.0 & 0.0 \\ -0.93 & 0.0 & 0.0 & 0.0 & 0.0 & 0.0 & 0.0 & 0.0 & 0.0 \\ 0.63 & -1.29 & 0.0 & 0.0 & 0.0 & 0.0 & 0.0 & 0.0 & 0.0 \\ 0.39 & -0.11 & -1.41 & 0.0 & 0.0 & 0.0 & 0.0 & 0.0 & 0.0 \\ -0.07 & -0.05 & 0.83 & -1.59 & 0.0 & 0.0 & 0.0 & 0.0 & 0.0 \\ 0.07 & -0.11 & 0.27 & 0.27 & -1.53 & 0.0 & 0.0 & 0.0 & 0.0 \\ -0.05 & 0.03 & 0.01 & 0.15 & 0.17 & -1.15 & 0.0 & 0.0 & 0.0 \\ -0.21 & 0.27 & -0.07 & -0.03 & 0.19 & 0.09 & -0.99 & 0.0 & 0.0 \\ -0.15 & 0.15 & 0.03 & -0.09 & 0.25 & 0.25 & 0.21 & -1.71 & 0.0 \end{bmatrix}$
10	$\begin{bmatrix} 0.0279 \\ 0.0479 \\ 0.0646 \\ 0.0659 \\ 0.1045 \\ 0.1066 \\ 0.1355 \\ 0.1622 \\ 0.1942 \\ 0.0908 \end{bmatrix}$	$\begin{bmatrix} 0.0 & 0.0 & 0.0 & 0.0 & 0.0 & 0.0 & 0.0 & 0.0 & 0.0 & 0.0 \\ -0.95 & 0.0 & 0.0 & 0.0 & 0.0 & 0.0 & 0.0 & 0.0 & 0.0 & 0.0 \\ 0.59 & -1.17 & 0.0 & 0.0 & 0.0 & 0.0 & 0.0 & 0.0 & 0.0 & 0.0 \\ 0.35 & -0.11 & -1.45 & 0.0 & 0.0 & 0.0 & 0.0 & 0.0 & 0.0 & 0.0 \\ -0.13 & 0.01 & 0.75 & -1.49 & 0.0 & 0.0 & 0.0 & 0.0 & 0.0 & 0.0 \\ 0.05 & -0.05 & 0.31 & 0.29 & -1.59 & 0.0 & 0.0 & 0.0 & 0.0 & 0.0 \\ 0.05 & -0.03 & -0.09 & 0.23 & 0.17 & -1.19 & 0.0 & 0.0 & 0.0 & 0.0 \\ -0.03 & 0.07 & -0.09 & -0.03 & 0.27 & -0.03 & -0.91 & 0.0 & 0.0 & 0.0 \\ -0.15 & 0.17 & 0.03 & -0.09 & 0.05 & 0.09 & 0.05 & -0.79 & 0.0 & 0.0 \\ -0.17 & 0.11 & 0.15 & 0.03 & 0.05 & 0.25 & 0.05 & -0.07 & -1.49 & 0.0 \end{bmatrix}$

J.2. Solver Searched on FlowDCN-B/2

NFE	TimeDeltas Δt	Coeffcients c_i^j
5	$\begin{bmatrix}0.0521\\0.1475\\0.2114\\0.2797\\0.3092\end{bmatrix}$	$\begin{bmatrix}0.0&0.0&0.0&0.0&0.0\\-1.26&0.0&0.0&0.0&0.0\\1.38&-2.26&0.0&0.0&0.0\\0.0&0.0&-0.92&0.0&0.0\\0.0&0.0&0.0&-0.7&0.0\end{bmatrix}$
6	$\begin{bmatrix}0.0391\\0.0924\\0.165\\0.2015\\0.2511\\0.2511\end{bmatrix}$	$\begin{bmatrix}0.0&0.0&0.0&0.0&0.0&0.0\\-1.22&0.0&0.0&0.0&0.0&0.0\\1.12&-2.0&0.0&0.0&0.0&0.0\\-0.3&0.9&-1.56&0.0&0.0&0.0\\0.0&0.0&0.0&-0.74&0.0&0.0\\0.0&0.0&0.0&0.0&-0.62&0.0\end{bmatrix}$
7	$\begin{bmatrix}0.0387\\0.0748\\0.103\\0.1537\\0.184\\0.234\\0.2117\end{bmatrix}$	$\begin{bmatrix}0.0&0.0&0.0&0.0&0.0&0.0&0.0\\-1.11&0.0&0.0&0.0&0.0&0.0&0.0\\1.03&-1.99&0.0&0.0&0.0&0.0&0.0\\0.07&0.43&-1.57&0.0&0.0&0.0&0.0\\-0.21&-0.15&1.53&-2.29&0.0&0.0&0.0\\-0.05&0.07&-0.23&0.61&-1.33&0.0&0.0\\-0.17&0.31&-0.41&0.17&0.59&-1.31&0.0\end{bmatrix}$
8	$\begin{bmatrix}0.0071\\0.0613\\0.078\\0.1163\\0.1421\\0.188\\0.2077\\0.1996\end{bmatrix}$	$\begin{bmatrix}0.0&0.0&0.0&0.0&0.0&0.0&0.0&0.0\\-2.43&0.0&0.0&0.0&0.0&0.0&0.0&0.0\\0.61&-1.55&0.0&0.0&0.0&0.0&0.0&0.0\\0.99&-0.11&-2.07&0.0&0.0&0.0&0.0&0.0\\0.05&-0.49&1.33&-1.93&0.0&0.0&0.0&0.0\\0.05&-0.33&0.23&0.73&-1.71&0.0&0.0&0.0\\-0.09&0.25&-0.29&0.05&0.61&-1.45&0.0&0.0\\-0.23&0.21&-0.01&-0.25&0.25&0.41&-1.25&0.0\end{bmatrix}$
9	$\begin{bmatrix}0.0017\\0.051\\0.0636\\0.0911\\0.1007\\0.1443\\0.1694\\0.191\\0.1872\end{bmatrix}$	$\begin{bmatrix}0.0&0.0&0.0&0.0&0.0&0.0&0.0&0.0&0.0\\-6.19&0.0&0.0&0.0&0.0&0.0&0.0&0.0&0.0\\-0.11&-0.81&0.0&0.0&0.0&0.0&0.0&0.0&0.0\\0.73&-0.17&-1.37&0.0&0.0&0.0&0.0&0.0&0.0\\0.31&-0.05&0.19&-1.45&0.0&0.0&0.0&0.0&0.0\\0.03&-0.23&0.29&0.35&-1.35&0.0&0.0&0.0&0.0\\-0.19&0.05&0.01&0.21&0.25&-1.23&0.0&0.0&0.0\\-0.23&0.21&-0.13&0.17&0.09&0.09&-1.09&0.0&0.0\\-0.17&0.15&0.11&-0.19&0.03&0.23&0.17&-1.21&0.0\end{bmatrix}$
10	$\begin{bmatrix}0.0016\\0.0538\\0.0347\\0.0853\\0.0853\\0.1198\\0.1351\\0.165\\0.1788\\0.1406\end{bmatrix}$	$\begin{bmatrix}0.0&0.0&0.0&0.0&0.0&0.0&0.0&0.0&0.0&0.0\\-7.8801&0.0&0.0&0.0&0.0&0.0&0.0&0.0&0.0&0.0\\-0.4&-0.74&0.0&0.0&0.0&0.0&0.0&0.0&0.0&0.0\\0.48&-0.18&-0.86&0.0&0.0&0.0&0.0&0.0&0.0&0.0\\0.26&-0.04&-0.04&-1.28&0.0&0.0&0.0&0.0&0.0&0.0\\0.0&-0.06&0.26&0.26&-1.42&0.0&0.0&0.0&0.0&0.0\\-0.1&-0.06&0.08&0.2&0.22&-1.24&0.0&0.0&0.0&0.0\\-0.18&0.14&-0.08&0.1&0.08&0.14&-1.06&0.0&0.0&0.0\\-0.12&0.16&-0.1&0.04&0.08&0.06&0.08&-1.02&0.0&0.0\\-0.16&0.02&0.14&0.0&-0.14&0.08&0.14&0.34&-1.38&0.0\end{bmatrix}$

J.3. Solver Searched on DiT-XL/2

NFE	TimeDeltas Δt	Coeffcients c_i^j
5	$\begin{bmatrix}0.2582\\0.1766\\0.1766\\0.2156\\0.1731\end{bmatrix}$	$\begin{bmatrix}0.0 & 0.0 & 0.0 & 0.0 & 0.0\\-1.43 & 0.0 & 0.0 & 0.0 & 0.0\\0.93 & -1.55 & 0.0 & 0.0 & 0.0\\0.0 & 0.0 & -0.69 & 0.0 & 0.0\\0.0 & 0.0 & 0.0 & -0.59 & 0.0\end{bmatrix}$
6	$\begin{bmatrix}0.2483\\0.1506\\0.1476\\0.1568\\0.1733\\0.1233\end{bmatrix}$	$\begin{bmatrix}0.0 & 0.0 & 0.0 & 0.0 & 0.0 & 0.0\\-1.36 & 0.0 & 0.0 & 0.0 & 0.0 & 0.0\\0.9 & -1.84 & 0.0 & 0.0 & 0.0 & 0.0\\-0.08 & 0.5 & -1.08 & 0.0 & 0.0 & 0.0\\0.0 & 0.0 & 0.0 & -0.56 & 0.0 & 0.0\\0.0 & 0.0 & 0.0 & 0.0 & -0.56 & 0.0\end{bmatrix}$
7	$\begin{bmatrix}0.2241\\0.1415\\0.1205\\0.1158\\0.1443\\0.1627\\0.0911\end{bmatrix}$	$\begin{bmatrix}0.0 & 0.0 & 0.0 & 0.0 & 0.0 & 0.0 & 0.0\\-1.38 & 0.0 & 0.0 & 0.0 & 0.0 & 0.0 & 0.0\\1.08 & -2.02 & 0.0 & 0.0 & 0.0 & 0.0 & 0.0\\-0.28 & 0.78 & -1.52 & 0.0 & 0.0 & 0.0 & 0.0\\-1.4901e-08 & -0.1 & 0.64 & -1.5 & 0.0 & 0.0 & 0.0\\0.06 & -0.06 & -0.06 & 0.26 & -1.0 & 0.0 & 0.0\\0.0 & -0.1 & 0.02 & 0.2 & 0.26 & -1.12 & 0.0\end{bmatrix}$
8	$\begin{bmatrix}0.2033\\0.1476\\0.1094\\0.099\\0.1116\\0.1233\\0.131\\0.0748\end{bmatrix}$	$\begin{bmatrix}0.0 & 0.0 & 0.0 & 0.0 & 0.0 & 0.0 & 0.0 & 0.0\\-1.14 & 0.0 & 0.0 & 0.0 & 0.0 & 0.0 & 0.0 & 0.0\\0.8 & -1.76 & 0.0 & 0.0 & 0.0 & 0.0 & 0.0 & 0.0\\0.02 & 0.48 & -1.62 & 0.0 & 0.0 & 0.0 & 0.0 & 0.0\\-0.12 & 0.06 & 0.62 & -1.42 & 0.0 & 0.0 & 0.0 & 0.0\\0.04 & -0.1 & 0.12 & 0.16 & -1.04 & 0.0 & 0.0 & 0.0\\0.06 & -0.04 & -0.06 & 0.08 & -0.08 & -0.56 & 0.0 & 0.0\\-0.02 & -0.04 & -0.04 & 0.12 & 0.14 & 0.04 & -0.9 & 0.0\end{bmatrix}$
9	$\begin{bmatrix}0.1959\\0.1313\\0.1142\\0.0863\\0.0898\\0.0916\\0.1119\\0.1054\\0.0735\end{bmatrix}$	$\begin{bmatrix}0.0 & 0.0 & 0.0 & 0.0 & 0.0 & 0.0 & 0.0 & 0.0 & 0.0\\-1.28 & 0.0 & 0.0 & 0.0 & 0.0 & 0.0 & 0.0 & 0.0 & 0.0\\0.78 & -1.62 & 0.0 & 0.0 & 0.0 & 0.0 & 0.0 & 0.0 & 0.0\\-0.02 & 0.44 & -1.48 & 0.0 & 0.0 & 0.0 & 0.0 & 0.0 & 0.0\\-0.1 & 0.16 & 0.36 & -1.3 & 0.0 & 0.0 & 0.0 & 0.0 & 0.0\\-0.06 & -0.04 & 0.22 & 0.12 & -1.08 & 0.0 & 0.0 & 0.0 & 0.0\\0.08 & -0.1 & -0.04 & 0.24 & -0.06 & -0.86 & 0.0 & 0.0 & 0.0\\0.04 & -0.04 & -0.04 & 0.0 & 0.06 & -0.08 & -0.5 & 0.0 & 0.0\\-0.04 & 0.0 & 0.0 & -0.02 & 0.14 & 0.02 & 0.0 & -0.74 & 0.0\end{bmatrix}$
10	$\begin{bmatrix}0.2174\\0.1123\\0.1037\\0.0724\\0.0681\\0.0816\\0.0938\\0.0977\\0.0849\\0.0681\end{bmatrix}$	$\begin{bmatrix}0.0 & 0.0 & 0.0 & 0.0 & 0.0 & 0.0 & 0.0 & 0.0 & 0.0 & 0.0\\-1.17 & 0.0 & 0.0 & 0.0 & 0.0 & 0.0 & 0.0 & 0.0 & 0.0 & 0.0\\0.35 & -0.99 & 0.0 & 0.0 & 0.0 & 0.0 & 0.0 & 0.0 & 0.0 & 0.0\\0.25 & -0.11 & -0.99 & 0.0 & 0.0 & 0.0 & 0.0 & 0.0 & 0.0 & 0.0\\0.03 & 0.05 & -0.07 & -0.85 & 0.0 & 0.0 & 0.0 & 0.0 & 0.0 & 0.0\\-0.03 & 0.03 & 0.25 & -0.09 & -0.93 & 0.0 & 0.0 & 0.0 & 0.0 & 0.0\\-0.01 & -0.03 & -0.01 & 0.21 & -0.11 & -0.67 & 0.0 & 0.0 & 0.0 & 0.0\\0.01 & -0.03 & -0.03 & 0.07 & 0.09 & -0.03 & -0.81 & 0.0 & 0.0 & 0.0\\0.03 & -0.03 & -0.03 & -0.03 & 0.05 & 0.01 & -0.11 & -0.27 & 0.0 & 0.0\\-0.01 & -0.01 & -0.01 & -0.01 & 0.03 & 0.07 & -0.01 & -0.05 & -0.57 & 0.0\end{bmatrix}$